

**Preliminary Parallaxes of 40 L and T Dwarfs from the
U.S. Naval Observatory Infrared Astrometry Program**

F. J. Vrba, A. A. Henden¹, C. B. Luginbuhl, H. H. Guetter, J. A. Munn, and B. Canzian

U.S. Naval Observatory, Flagstaff Station, P.O. Box 1149, Flagstaff, AZ 86002-1149

*fjv@nofs.navy.mil, aah@nofs.navy.mil, cbl@nofs.navy.mil, guetter@nofs.navy.mil,
jam@nofs.navy.mil, blaise@nofs.navy.mil*

A. J. Burgasser²

*University of California, Los Angeles, Division of Astronomy and Astrophysics,
405 Hilgard Ave., Los Angeles, CA 90095-1562*

adam@astro.ucla.edu

J. Davy Kirkpatrick

*California Institute of Technology, IPAC,
770 S. Wilson Ave., MS 100-22, Pasadena, CA 91125*

davy@ipac.caltech.edu

X. Fan

Steward Observatory, The University of Arizona, 933 N. Cherry Ave., Tucson, AZ 85721

fan@as.arizona.edu

T. R. Geballe

Gemini Observatory, 670 N. A'ohoku Place, Hilo, HI 96720

tgeballe@gemini.edu

D. A. Golimowski

*Department of Physics and Astronomy, The Johns Hopkins University
3400 N. Charles St., Baltimore, MD 21218*

dag@pha.jhu.edu

G. R. Knapp

Department of Astrophysical Sciences, Princeton University, Princeton, NJ 08544

gk@astro.princeton.edu

S. K. Leggett

*United Kingdom Infrared Telescope, Joint Astronomy Centre,
660 N. A'ohoku Place, Hilo, HI 96720*

s.leggett@jach.hawaii.edu

D. P. Schneider

*Pennsylvania State University, Department of Astronomy and Astrophysics,
525 Davey Lab., University Park, PA 16802*

dps@astro.psu.edu

and

J. Brinkmann

Apache Point Observatory, P.O. Box 59, Sunspot, NM 88349-0059

jb@apo.nmsu.edu

ABSTRACT

We present preliminary trigonometric parallaxes and proper motions for 22 L dwarfs and 18 T dwarfs measured using the ASTROCAM infrared imager on the U.S. Naval Observatory (USNO) 1.55-m Strand Astrometric reflector. The results presented here are based on observations obtained between September 2000 and November 2002; about half of the objects have an observational time baseline of $\Delta t = 1.3$ yr and half $\Delta t = 2.0$ yr. Despite these short time baselines, the astrometric quality is sufficient to produce significant new results, especially for the nearer T dwarfs. Seven objects are in common with the USNO optical CCD parallax program for quality control and seven in common with the ESO 3.5-m NTT parallax program. We compare astrometric quality with both of these programs. Relative to absolute parallax corrections are made by employing 2MASS and/or SDSS photometry for reference frame stars. We combine USNO infrared and optical parallaxes with the best available CIT system photometry to determine M_J , M_H , and M_K values for 37 L dwarfs between spectral types L0 to L8 and 19 T dwarfs between spectral types T0.5 and T8 and present selected absolute magnitude versus spectral type and color diagrams, based on these results. Luminosities and temperatures are estimated for these objects. Of special interest are the distances of several objects

¹Universities Space Research Association

²Hubble Fellow

which are at or near the L–T dwarf boundary so that this important transition can be better understood. The previously reported early-mid T dwarf luminosity excess is clearly confirmed and found to be present at J, H, and K. The large number of objects that populate this luminosity excess region indicates that it cannot be due entirely to selection effects. The T dwarf sequence is extended to $M_J \approx 16.9$ by 2MASS J041519–0935 which, at $d = 5.74$ pc, is found to be the least luminous [$\log(L/L_\odot) = -5.58$] and coldest ($T_{\text{eff}} \approx 760$ K) brown dwarf known. Combining results from this paper with earlier USNO CCD results we find that, in contrast to the L dwarfs, there are no examples of low velocity ($V_{\text{tan}} < 20 \text{ km s}^{-1}$) T dwarfs. This is consistent with the T dwarfs in this study being generally older than the L dwarfs. We briefly discuss future directions for the USNO infrared astrometry program.

Subject headings: astrometry — color-magnitude diagrams — stars:distances — stars:late-type — stars: low-mass, brown dwarfs

1. Introduction

After the era of photographic proper motion surveys (e.g. Luyten 1979) revealed late M stars close to the limit of stellar hydrogen burning, a long, and largely frustrating, pursuit of sub-stellar objects was begun by many researchers. These efforts were motivated by the overarching desire to understand the Galactic mass and luminosity distributions of putative objects that would bridge the gap between the lowest mass stars and giant planets and by the fact that no theory of star formation could be considered complete without accounting for the mass function of such objects. Becklin & Zuckerman (1988) identified GD 165B as the first object clearly cooler than an M dwarf, followed several years later by the discovery of the first ‘methane dwarf’, Gliese 229B (Nakajima et al. 1995; Oppenheimer et al. 1995); an object cold enough that its spectrum shows strong methane absorption, similar to the giant gas planets. These ‘brown dwarfs’ became the prototypes for L dwarfs (Kirkpatrick et al. 1999; Martín et al. 1999) and T dwarfs (Burgasser et al. 2002a; Geballe et al. 2002), respectively.

It was not, however, until deep, large-scale optical surveys (the Sloan Digital Sky Survey [SDSS]¹; York et al. 2000; Abazajian et al. 2003) and near-infrared surveys (the Two Micron All Sky Survey [2MASS]²; Skrutskie et al. 1997) and the Deep Near Infrared Survey of the Southern Sky [DENIS³; Delfosse et al. 1997, Epchtein 1997]) of the sky were undertaken that significant numbers of field brown dwarfs were revealed. L dwarfs from these surveys have been identified by many authors (Delfosse et al. 1997; Kirkpatrick et al. 1999; Kirkpatrick et al. 2000;

¹www.sdss.org

²www.ipac.caltech.edu/2mass

³cdsweb.u-strasbg.fr/denis.html

Fan et al. 2000; Hawley et al. 2002; Geballe et al. 2002; Schneider et al. 2002), as have T dwarfs (Burgasser et al. 1999; Strauss et al. 1999; Tsvetanov et al. 2000; Leggett et al. 2000; Burgasser et al. 2002a; Geballe et al. 2002; Burgasser et al. 2003a; Knapp et al. 2004), amongst many others. Comprehensive summaries of field brown dwarf discoveries are maintained at the web sites maintained by Kirkpatrick for L dwarfs (spider.ipac.caltech.edu/staff/davy/ARCHIVE), by Burgasser for T dwarfs (www.astro.ucla.edu/adam/homepage/research/tdwarf), and by Leggett for both L and T dwarfs (www.jach.hawaii.edu/skl/LTdata.html). Currently there are more than 250 L dwarfs and 58 T dwarfs known.

Unlike stars, brown dwarfs are not massive enough to sustain continuous hydrogen fusion in their cores, but cool continually from their birth. Somewhere between early and mid-L is the crossover between hydrogen-burning stars and brown dwarfs. Unfortunately, other than objects in clusters (Basri 2000), it is difficult to establish ages for brown dwarfs, since their spectra do not always exhibit a known direct indicator of age such as from Li destruction. This results in degeneracies amongst mass, age, and luminosity. However, for all but the youngest objects, brown dwarf radii are largely independent of mass and age, and all are similar to the radius of Jupiter (Chabrier & Baraffe 2000). Thus luminosity scales well with T_{eff}^4 , with L dwarfs having surface temperatures in the range 2200–1400 K, while T dwarfs have temperatures down to about 700 K (e.g. Kirkpatrick et al. 2000; Leggett et al. 2001; Leggett et al. 2002; Dahn et al. 2002; Burgasser et al. 2002a; Golimowski et al. 2004; this paper). Obviously, an accurate measurement of the distances to these objects is required to determine their luminosities and temperatures, along with understanding many other issues such as their cooling curves and surface flux redistribution due to atmospheric dust formation.

In earlier work, U.S. Naval Observatory (USNO) optical CCD parallaxes and proper motions were presented for eight late M dwarfs, 17 L dwarfs, and three T dwarfs (Dahn et al. 2002, hereafter D02). Most recently Tinney, Burgasser, & Kirkpatrick (2003, hereafter TBK03) presented near-infrared parallaxes and proper motions of 9 T dwarfs. In this paper we present preliminary trigonometric parallaxes and proper motions, obtained at near-infrared wavelengths, of 22 L dwarfs and 18 T dwarfs plus four additional L or T dwarf companion objects in binaries. We feel compelled to present preliminary parallaxes and proper motions now due to the intense interest by the community in distance determinations to these objects, rather than waiting approximately another two years of observational time baseline before final results would be available for most of the objects. Final results will be presented in later papers.

2. Development of Near-Infrared Astrometric Capabilities at USNO

In the mid-1990s USNO anticipated a need to have the capability of carrying out high accuracy relative astrometry at near-infrared wavelengths. This was based on the possibility that results from the upcoming 2MASS, DENIS, and SDSS sky surveys might reveal large numbers of brown dwarfs and other cool and dust-embedded objects which would be better detected in the near-infrared

than at visible wavelengths. This need was also consistent with the USNO mission of testing the astrometric capabilities of new technology array detectors and extending this investigation to longer wavelengths. While the near-infrared offered the prospects of better detection for cool objects with smaller differential color refraction and somewhat better seeing than in the optical, the effects on astrometry of telescope and variable sky background radiation, along with the additional infrared camera optics needed to apodize emissive telescope parts and the performance of infrared array detectors themselves, were not known. Astrometric testing was carried out between 1995 and 1999 at USNO using a Rockwell HgCdTe 256^2 (NICMOS-II) array in a camera not optimized for astrometric work. Repeated observations were obtained during this time frame of stars in the clusters M67 and NGC 7790 with J,H,K magnitudes between about 11 and 14. For observations with seeing ≤ 1.5 arcsec, we found mean errors of unit weight for a single observation of 7, 10, and 11 milli-arcseconds (mas) for J, H, and K, respectively (Vrba et al. 2000). These results, while not as good as those obtained with CCDs (Dahn 1997), encouraged us to pursue instrumentation specifically designed for carrying out a routine astrometric program in the near-infrared.

A major problem encountered was that, at reasonable pixelization, 256^2 format devices offer fields of view which typically are not large enough to present an adequate reference frame. Thus, in 1993 USNO joined with partner institution the National Optical Astronomical Observatories to fund the development of the ALADDIN 1024^2 InSb array detector (Fowler et al. 1996) at Santa Barbara Research Corporation (now Raytheon Vision Systems). This partnership led to the successful development of ALADDIN arrays, which are now used throughout astronomy. In 1996 USNO and the Naval Research Laboratory jointly began designing an ALADDIN-based camera. Mauna Kea Infrared (MKI) was contracted to build this camera, known as ASTROCAM, which was delivered to the USNO, Flagstaff Station in August 1999. For 20 months ASTROCAM was operated with an engineering grade detector, during which time we optimized operation of the camera and developed an operational plan for making brown dwarf astrometric observations. In April 2000 a science grade ALADDIN array was installed, and in September 2000 the full parallax and proper motion program for brown dwarfs was initiated.

3. Instrumentation

ALADDIN array detectors (Fowler et al. 1996) have $27 \mu\text{m}$ pixels with essentially 100% fill factor and approximately 85% quantum efficiency between 0.9 and $5 \mu\text{m}$. The array is designed with quadrant architecture and eight outputs per quadrant. The particular array which we employ in ASTROCAM has dark current of about $0.7 \text{ e}^- \text{ sec}^{-1}$ at its operating temperature of 30 K and has a full well capacity of about $2.1 \times 10^5 \text{ e}^-$ at its operating -0.8 volt bias level. With double correlated sampling we obtain a read noise of about 30 e^- RMS. Except for an avoided region near one edge, which was over-thinned during fabrication and which covers about 3% of the area of the array, our device has pixel operability of $> 99.99\%$.

ASTROCAM was delivered by MKI as a turnkey system including DSP-based electronics and

a graphical user interface and is used exclusively at the 1.55-m Kaj Strand Astrometric Reflector at the USNO, Flagstaff Station. Since one of ASTROCAM's missions is astrometric measurements, its structure was designed to minimize flexure. The heart of ASTROCAM is an all-reflective Offner 1:1 re-imaging system, which eliminates refractive optics except for the entrance window and filters, which are tilted at 5° to avoid production of ghost images. Thus the ALADDIN $27\ \mu\text{m}$ pixels are at the natural telescope scale providing 0.3654 arcsec pixelization and a field of view of about 6.2×6.2 arcmin. Determination of the pixel scale was accomplished by observation of stellar clusters with well-determined astrometric positions. Pupil plane apodization of the telescope structure is accomplished via a mask deposited on the secondary mirror of the Offner re-imager for the outside edge of the optics and a light trap cone to mask the telescope primary mirror central hole. The telescope secondary support struts are not apodized. The system is telecentric so that mis-focus does not change the focal plane scale. The Offner system provides image spot sizes of less than 0.5 pixel even at the very corners of the array. Field distortion has been measured, by observation with ASTROCAM of astrometric calibration fields made with the Flagstaff Astrometric Scanning Transit Telescope (FASTT; Stone 1997), at less than 100 mas RMS over the entire field, a number which is dominated by the FASTT astrometric accuracy. Two 10-position concentric filter wheels currently house seven broadband filters (Z, J, H, K, K', K-long, L') and nine narrow-band astrophysical filters, plus a cold blank position. An extensive description of the ASTROCAM system is given by Fischer et al. (2003).

4. Observational Procedures

ASTROCAM is scheduled on the 1.55-m telescope from 11 to 14 nights each lunation during bright time. Approximately 75% of the scheduled time is used for observations on the infrared parallax and proper motion program. Observations are carried out under seeing conditions up to 2.5 arcsec FWHM, although, in practice, the exposure times get prohibitively long for some of the fields at 2.5 arcsec. Despite the fact that differential color refraction (DCR) in the near-infrared is smaller than in the optical, we continue the CCD parallax program practice of only obtaining observations as objects cross the meridian. Because of this, we do not apply DCR corrections, although we may consider testing DCR corrections on some fields in the future.

Prior to starting our parallax program we carried out test astrometric observations of several L and T dwarfs in the J, H, and K bands. Best results were obtained when L dwarfs were observed in H band and T dwarfs in J band, reflecting the highest signal-to-background noise ratio for each kind of object. With the exception of two objects, noted below, we continue to observe T dwarfs in J band and L dwarfs in H band.

Exposure times are set by the desire to not saturate either the parallax object or reference frame stars and range from 30 to 60 seconds, with the number of coadds under nominal conditions ranging from 8-20, with approximately twice as many coadds employed under the most marginal conditions. A typical integration time for a single telescope dithered position is 10 minutes in

nominal conditions and 20 minutes for a faint field under poor conditions. These relatively long exposure times are necessary because the 1.55-m telescope has a small effective aperture due to its large secondary mirror. Since our total integration times for a given field can range from 20 to 60 minutes, all exposures are guided by an optical wavelength leaky guider. These relatively long exposure times are another reason why we do not obtain observations off the meridian, since the large DCR between the infrared imaging and optical guiding would be transferred to the infrared images.

Three dithered integrations are obtained for each observation. The dither offset between positions is 10 arcsec, with the dither pattern being north–south or east–west around the nominal position, depending on the distribution of the reference frame stars. The nominal registration of each field is repeated to within a few pixels for each visitation of a field. We have chosen to stay with a minimum number of dithers based on our tests which show that astrometric quality is not affected by pixel sampling even under the best seeing conditions we experience.

5. Data Processing and Astrometric Reduction Procedures

The data processing procedures are again a product of extensive testing of astrometric solutions with ASTROCAM during the period before the astrometric program began. The first step is that all frames used in processing, program and flats, are linearized via a process similar to that described by Luginbuhl et al. (1998) for our earlier NICMOS-II device. Linearization improves the astrometric centroiding somewhat since it has the effect of slightly sharpening the image profile. After linearization all program frames are flat–fielded. We use dome flats, which are composed of the difference frames of three dome flat screen illuminated and unilluminated sets. The difference frames are median combined into a single flat–field frame for each filter employed. After flat–fielding, the program frames are passed through a min/max value filter to construct a sky frame which is subtracted from each program frame.

Astrometry is performed on individual program frames, processed as described above, not on combined frames. Centroiding for the parallax target object and the reference frame stars is accomplished via a two dimensional Gaussian fit technique (Monet & Dahn 1983), which is also employed in the USNO optical CCD parallax program. The astrometric solutions are determined via the techniques and software developed by D. G. Monet (Monet & Dahn 1983; Monet et al. 1992) which are again borrowed from the USNO optical program and modified for use in our infrared program to accommodate such factors as highly varying net backgrounds. As in the optical CCD program, we use only linear frame constants and allow frame scale and rotation to be free parameters. (In fact, we do solve for second and third order frame constants, but discard them as they are always trivial compared to their solution errors.) All reference stars used in the reference frame are given unit weighting.

6. What is Meant by ‘Preliminary’ Astrometric Results?

There are several considerations which make the parallax and proper motion results we present in this paper ‘preliminary’ rather than final. While our observing program is continuing, due to the intense interest in brown dwarfs, we decided to use the observations in hand at the end of the November 2002 observing run to provide these preliminary astrometric results. Since observations were initiated in September 2000, this meant that about half of the fields had been observed for a time baseline Δt of about 2.0 years and about half for only 1.3 years. Normally we would allow a minimum three years of observing to allow uniform coverage of the observable part of the parallactic ellipse, add time baseline to the proper motion determinations, add to \sqrt{n} statistics, and have a complete separation of parallax from proper motion solutions.

Second, the parallax results we report here are only for the X (right ascension) solutions and do not include the Y (declination) solutions weighted by error. The astrometric errors we find for ASTROCAM are nearly as good in Y as they are in X (see §11) and, of course, we have to employ both X and Y astrometry to derive proper motions. However, since the parallactic ellipse is a circle at the ecliptic pole and a line in the ecliptic plane, the Y parallax determination is always worse than the X determination except at the pole. Thus, Y parallax solutions with the short Δt as of November 2002 range from having internal S/N of 10 down to 1. Rather than publishing combined values for only those cases for which the Y determination helped the solution, we feel that it is more straightforward to publish the X-determined solutions at this time. When we publish final parallaxes we will present fully combined X and Y solutions.

Third, we are not employing the best astrometric reference frames for our preliminary solutions. The reference frames we use here are based on those stars for which we have adequate optical and/or infrared photometry to determine a photometric parallax for use in determining the correction from relative to absolute parallax for each frame (see §9 on absolute parallax corrections). Naturally, it is best to use as many stars as possible which are well distributed over the field to produce the most robust reference frame. For most fields we have at least some stars which serve as otherwise excellent reference frame stars, but for which we do not have adequate photometry, and thus they cannot be employed in our solution. Although it is the case that the corrections from relative to absolute parallax are typically dwarfed by the parallaxes of these objects, it is not formally correct to include reference stars for which we have no photometric parallaxes. It is one of our goals to obtain the necessary photometry in order to employ the best possible reference frames when we publish final parallaxes.

Finally, we have not solved for nor culled any stars in the reference frames which might have measurable proper motions. This should have no effect on the parallax solutions, since parallax and proper motion solutions are largely orthogonal and should have minimal effect on proper motions since there are numerous reference frame stars used in each solution. Mostly this will have the effect of increasing the apparent errors of our global frame solutions (see §11 on astrometric quality).

Despite these shortcuts, the preliminary parallax and proper motions we present here agree

with the previously published results for objects in common and produce relatively tight spectral type – absolute magnitude diagrams. We are confident that our results are significant to within the errors we publish. Nonetheless, we caution that these are preliminary results.

7. Objects on the Program

In Table 1 we list the full designations of the 40 L and T dwarfs or multiple systems with which we began our initial near-infrared parallax program in September 2000 and for all of which we are reporting preliminary results. Hereafter, we use an abbreviated designation for each object. There are, in fact, 44 L and T dwarfs for which we have parallactic information as four of the objects (2MASS J085035+1057AB, 2MASS J122554–2739AB, 2MASS J172811+3948AB, and 2MASS J210115+1756AB) are known doubles, which we discuss later. The 40 initial objects were selected primarily to complement those which were already being observed on the USNO optical parallax program. Specifically, this meant an emphasis on T dwarfs and a selection of late L dwarfs, all of which were difficult to observe with optical CCDs. Twenty two of the objects are L dwarfs and 18 are T dwarfs. Seven objects (2MASS J055919–1404, 2MASS J082519+2115, 2MASS J085035+1057, SDSS J125453–0122, SDSS J162414+0029, 2MASS J163229+1904, and 2MASS J222443–0158) were chosen to be observed in parallel with the USNO optical program in order to provide independent determinations of parallaxes and proper motions and to serve as quality control for both programs. Some of the objects had already been published at the time we began our program, while others were provided to us by members of the 2MASS and SDSS teams as part of the USNO collaboration in these surveys. Twenty two of the objects are from the 2MASS survey, while 18 are from the SDSS survey. Column two of Table 1 provides the adopted spectral type from the literature (see §13).

Column 3 of Table 1 gives the broadband filter (J or H) in which the astrometry is done for these objects. Note that, contrary to our methodology described above (that we observe L dwarfs in the H filter and T dwarfs in the J filter), two of the objects (SDSS J015141+1244 and SDSS J020742+0000) are T dwarfs being observed in the H filter. This is due to the fact that at the time we started observations they were thought to be L dwarfs, but were later determined to be T dwarfs. Rather than starting a new series of observations we decided to simply continue the observations in the H filter, although at the expense of optimal detection S/N.

Columns 4 and 5 give the number of nights on which each object has been observed and the timespan over which the observations have been taken, respectively. The 18 objects between right ascension 10^h and 18^h have been observed for an average of 21.2 nights and an average timespan of 1.34 years, while those between right ascension 18^h and 10^h have been observed for an average of 26.7 nights but with a significantly longer average elapsed time of 2.03 years. This is an artifact of our decision to use data taken through the observing run of November 2002 as the preliminary database.

Column 6 gives the mean epoch of the observations for each object. Column 7 gives the number of reference frame stars employed in the solution, while column 8 gives a code describing how the conversion from relative to absolute parallax was determined for each reference frame, as explained in §9.

8. Reference Frame Selection

Registration of the parallax fields was determined by taking several test exposures and choosing a registration that left as many potential reference frame stars in the field of view of the array, but left the parallax target object as close to the field center as possible. Once observations were begun, a few processed frames with the best seeing available were inspected to rule out any extended objects or double stars as potential reference frame members. When adequate time had elapsed so that running astrometric solutions were practical, solutions were started using the full potential reference frame and stars identified as degrading the solution were discarded. The stars removed were typically significantly fainter than the mean reference frame brightness or very near the edge of the array. Finally, stars that did not have adequate photometry from which a photometric parallax could be determined were removed, as discussed above. Since we consider the reference frames used for these preliminary results to be provisional, we will defer, until such time as we publish final parallax results, a full discussion of the reference frames employed, including identification and magnitude range.

9. Relative to Absolute Parallax Corrections

Although the target objects of this program are nearby, we nevertheless determined corrections from relative to absolute parallaxes via photometric parallaxes for the reference frame stars using optical photometry from SDSS and/or infrared photometry from 2MASS. In all cases, photometric parallaxes were derived assuming that reference frame stars are main-sequence dwarfs. We used dereddened (using the extinction maps of Schlegel, Finkbeiner, & Davis 1998) SDSS colors for those reference frame stars with SDSS photometry (2MASS J121711–0311, 2MASS J123739+6526, 2MASS J171145+2232, and all SDSS fields except SDSS J042348–0414 and SDSS J053952–0059, which lie outside the official SDSS coverage). Since the average reference frame star distance is ≈ 630 pc (1.59 mas, see below) we applied the full thin disk reddening of the Schlegel, Finkbeiner, & Davis (1998) maps. For red stars ($i - z > 0.5$) we used the M_i vs. $i - z$ calibration of Hawley et al. (2002). For blue stars ($i - z < 0.5$) we used the M_R vs. $R - I$ calibration of Siegel et al. (2002). $r - i$ colors were transformed to $R - I$ colors using the transformations given by Smith et al. (2002). r magnitudes were transformed to R magnitudes using the equation $R = r - 0.21(r - i) - 0.17$ (D. Tucker, private communication). Only those blue stars in the color range $0.3 < R - I < 1.5$ had photometric parallaxes derived. This is slightly bluer than the range adopted by Siegel et al. (who used a blue cutoff of 0.4); the calibration still fits the dwarf sequence to $R - I = 0.3$, though

confusion with turnoff stars becomes greater.

For fields without SDSS photometry, but with 2MASS photometry, we transformed the 2MASS $J - H$ and $H - K$ colors to California Institute of Technology (CIT) colors (Elias et al. 1982) using the transformations of Carpenter (2001). The transformed colors were used to estimate spectral types from the spectral type versus infrared color calibration (transformed to the CIT system) of Bessell & Brett (1988). Absolute V magnitudes as a function of spectral type were taken from Schmidt-Kaler (1982) and converted to M_J and M_K via the Bessell & Brett (1988) calibrations. Distances were determined by averaging $(m - M)_J$ and $(m - M)_K$. Since extinction in the J - and K -bands is only a small fraction of that in the optical, reddening in the infrared was ignored. For the fields for which both SDSS and 2MASS colors were available, the average distance was taken. Column 7 of Table 1 gives the codes H, S, or IR indicating whether the Hawley et al. (2002), Siegel et al. (2002), and/or infrared calibrations were employed.

Since we give each reference frame star equal weight in the astrometric solution, the distances in milli-arcseconds (mas) for each star are simply averaged and a standard deviation of the mean calculated for each reference frame. The reference frame distances in mas are added to the relative parallax astrometric solutions in mas and the errors of the reference frame distance corrections are added in quadrature to the relative parallax astrometric errors. The average correction to absolute parallax is 1.59 mas, with average uncertainty 0.31 mas, and scatter 0.46 mas (std dev). The average correction for the 16 fields observed in the J filter is 1.70 mas, while for the 24 fields observed in the H filter it is 1.52 mas.

The mean ratio of $\Delta\pi_{rel \rightarrow abs} / \pi_{abs}$ is 0.036 ± 0.026 indicating that the mean correction adds only a few percent to the distance of these objects. The mean ratio of $\sigma(\Delta\pi_{rel \rightarrow abs}) / \sigma(\pi_{rel})$ is 0.087 ± 0.059 , indicating that the error of the corrections to absolute parallax, when added in quadrature, adds almost nothing to the total parallax error. The mean ratio of $\sigma(\Delta\pi_{rel \rightarrow abs}) / \pi_{abs}$ is 0.008 ± 0.014 , confirming that the error of the relative to absolute parallax correction is small compared to the parallaxes themselves for these objects.

Finally, we note that there are 76 reference frame stars distributed among 12 fields for which $\Delta\pi_{rel \rightarrow abs}$ was based on both SDSS optical and 2MASS infrared photometry. The mean difference between these (SDSS - 2MASS) is $+0.10 \pm 0.08$ (std dev mean) mas. Thus, there is no significant systematic difference in the reference frame distances estimated from SDSS and 2MASS.

10. Astrometric Results

Table 2 presents our preliminary proper motion and parallax results. The first column gives an abbreviated object name. The second column gives the spectral type which we adopt (see §13). The third column gives the parallax (π) solution relative to the reference frame employed along with the standard mean error. The fourth column gives the absolute parallax, which is corrected for the estimated distances to the reference frame stars as described in §9, along with its standard

mean error. The error for the absolute parallaxes contains, in quadrature, the sum of the error of the relative parallax determination with the error of the absolute parallax correction. Comparing the relative and absolute parallaxes and their errors demonstrates the small effect of the distance of the reference frame for these relatively nearby objects. The fifth column gives the relative proper motion (μ) in mas yr^{-1} with respect to the reference frame along with the formal uncertainty. The sixth column gives the position angle of the proper motion (in the sense east of north) along with its uncertainty. Using SDSS astrometric stars in the field for SDSS J053952–0059 for 41 frames spaced over two years we found the mean rotation of the field as -0.044 ± 0.063 deg. Thus, the natural rotation of ASTROCAM, when pointed at the meridian and $\delta \approx 0^\circ$, is indistinguishable from the celestial system, so we have made no rotation correction to the natural position angle. Finally, in the last column we give the tangential velocity with respect to the Sun by combining the absolute parallax and relative proper motion results.

11. Astrometric Quality

For the group of 18 objects with an average 21.2 nights and average $\Delta t = 1.34$ yr, the mean parallax error is 4.86 mas and the mean proper motion error is 8.23 mas yr^{-1} . For the group of 22 objects with an average 26.7 nights and average $\Delta t = 2.03$ yr, the mean parallax error is 3.86 mas and the mean proper motion error is 5.20 mas yr^{-1} . Thus the proper motion errors scale with $(\Delta t)^{-1}$ as might be expected if the observations are uniformly distributed. The parallax errors reduce somewhat faster than if proportional to $(\text{nights})^{-1}$. The most likely reason for this is that the objects with the smaller time baseline do not as yet have observations well distributed over parallax factor. Certainly the objects with only 1.34 yr of observations must be viewed with some degree of caution in this regard, although the spectral type versus absolute magnitude figures discussed below would indicate that there are no gross errors for any object. While we have chosen to not present the Y (declination) parallax results at this time, we note that the slope $\pi(Y)/\pi(X)$ is 0.99 ± 0.05 and that the $\pi(X)$ and $\pi(Y)$ results for all objects agree to within their error bars.

As Monet et al. (1992) have pointed out, the mean error for a single observation of unit weight (m.e.1) for an ensemble of stars on frames taken over a period of time is a useful measure of astrometric accuracy. They report a range of 3 to 5 mas as characteristic of fields observed in the USNO CCD parallax program on the 1.55-m telescope. For our preliminary data we find mean errors and standard deviations in X and Y, respectively, of 15.5 ± 4.9 and 17.9 ± 4.9 mas (8.9 ± 2.8 and 10.3 ± 2.9 mas for dithered triplets which are equivalent to one CCD observation). There is no significant difference between fields observed in J or H. These results improve considerably when solutions are run using only the four brightest reference frame stars with X and Y errors, respectively, of 8.1 ± 3.4 and 10.0 ± 4.1 (4.6 ± 1.9 and 5.8 ± 2.4 for dithered triplets). There is no obvious reason why the Y errors are systematically larger than X.

There are several likely reasons why the infrared astrometric accuracies are somewhat worse than for CCD results at the same telescope. The first is that we have thus far not solved for proper

motions for any of the reference frame stars. While largely orthogonal to the parallax solution, allowing for proper motions in the reference frame should significantly reduce m.e.1. Second, we have not made corrections for DCR, although, since our observations are in the infrared and are constrained to the meridian, we believe this has little effect. A third issue is the quality of some frames we have had to employ to produce a preliminary set of results. Figure 1 shows the histogram of seeing at the beginning of each set of observations employed in this paper. Although the median image size is 1.33 arcsec (FWHM), we have had to employ many frames with much worse seeing. Experience from the USNO CCD program has shown that astrometric quality is not significantly degraded when exposure times are increased by (image size)² so as to maintain a central image density. However, due to the small effective aperture of our telescope, our exposure times are typically 30 minutes for three dithers even in the best seeing. Thus, we can afford to only double exposure times in worse seeing. While the poorer seeing frames, at this point, help the parallax solution, they clearly hurt the m.e.1 statistics. As we accumulate more data over a longer time baseline the poorer seeing observations will be retired.

It is instructive to compare our infrared astrometric accuracy with that found by TBK03. Using the European Southern Observatory (ESO) 3.5-m New Technology Telescope (NTT) with 0.815 arcsec FWHM median seeing, they find an m.e.1 of 12.1 mas (0.042 pixel) for each 2 minute individual frame. From above we find an XY-averaged m.e.1 of 16.7 mas (0.046 pixel) for each typical 10 minute individual frame using a 1.55-m telescope with 1.33 arcsec FWHM median seeing.

12. Comparison of π and μ to Previous Results

12.1. USNO CCD Program

Table 3 compares the results for the seven objects in common between the USNO infrared and optical CCD programs (D02). Column 1 gives the abbreviated object names, the second column whether CCD, IR, or difference values, and the third column the range of time (ΔT) over which the observations were observed. The fourth column gives the derived absolute parallaxes, errors, and differences. While it is true that the CCD and IR parallaxes are derived using different reference frames, correction to absolute parallax should give consistent results. The fifth and sixth columns give the relative proper motions and position angles of proper motion and their errors, respectively, along with differences.

There are two objects that have marginally different parallaxes. One is 2MASS J085035+1057, which is a binary of 0.16 arcsec separation (Reid et al. 2001, discussed in §15.4) and for which the IR and CCD programs also derive marginally different proper motion position angles. Using our IR parallax, 0.16 arcsec semi-major axis, and the maximum mass of the system (Reid et al. 2001) we estimate a minimum orbital period of the system of ≥ 51 yr. Given the short ΔT s of both programs it is unlikely that orbital motion of the system could lead to major errors in the parallax or proper motion determinations. Also, our analysis in §15.4 indicates similar spectral types for

the two binary members, so that the photometric barycenters should not be strongly affected in either the optical or infrared. More observations in both programs will be needed of this system to ensure that the derived parallax is without systematic errors.

The second object with marginally different parallaxes is SDSS J125453–0122. There is no indication that this object is in a binary system. We see in §12.2 that the USNO IR parallax is nearly identical with that measured by TBK03, so we favor the USNO IR parallax over the USNO CCD parallax. (We note that the USNO optical measurement is based on only $\Delta T = 1.2$ yr, so the discrepancy may just be due to a small ΔT .)

The last line of Table 3 gives the weighted mean differences in parallax, proper motion, and proper motion position angle between the USNO IR and CCD determinations. There is no strong evidence for any systematic differences in these quantities determined between the two programs.

12.2. ESO 3.5-m NTT Infrared Program

Earlier (§11) we discussed the differences in astrometric quality between the USNO infrared program and the infrared program that has been carried out at the ESO 3.5-m NTT (TBK03). Table 4 compares the parallax and proper motion results for the seven objects in common between the infrared programs at USNO and at ESO. Column 1 gives the abbreviated object names, the second column whether USNO, ESO, or difference values, and the third column the range of time (Δt) over which the observations were obtained. Since TBK03 did not apply corrections to absolute parallax, in the fourth column we compare relative parallaxes and their errors. The fifth and sixth columns give the relative proper motions and position angles of proper motion and their errors, respectively.

One of the objects, 2MASS J122554–2739AB, is in a binary system (see §15.6); however, there is no significant difference between the parallaxes, proper motions, and position angles determined by both programs. The only marginally significant differences are for both the parallax and proper motion of 2MASS J104753+2124 and the parallax of 2MASS J121711–0311. It is not possible to understand which determination is better at this time, although we note that, for this object and all others in Table 4, the USNO observations are all in the shorter time baseline group of $\Delta t \approx 1.3$ yr.

The last line of Table 4 gives the weighted mean differences in parallax, proper motion, and proper motion position angle between the USNO and ESO determinations. There is no evidence for any systematic differences in these quantities determined between the two programs.

13. Adopted Spectral Types and Infrared Photometry

We compile here the spectral types and infrared photometry, primarily from the literature, to be used in the ensuing discussion. In Table 5 we present a small amount of USNO infrared

photometry relevant to the objects discussed in this paper. The data are an addendum to the USNO photometry obtained with IRCAM presented by D02 which gives details of the observations and reductions. These data are essentially on the CIT photometric system as they were obtained by normalization to the Elias et al. (1982)–based standards of Guetter et al. (2003). The exceptions to this are the data for SDSS J020742+0000, for which we used 2MASS All-Sky Point Source Catalog (PSC) photometry of stars within the field of view of ASTROCAM, converted those to CIT system values via the transformations of Carpenter (2001), and used instrumental ASTROCAM *JHK* magnitudes to obtain *JHK* photometry for this object. This process was adopted because 2MASS did not obtain photometry for this faint object and there are no published empirical transformations between photometry on other systems and the CIT system for T dwarfs. Stephens & Leggett (2004) have published synthetic transformations but in this paper we chose to employ empirical transformations only (see below).

In Table 6 we present adopted spectral types and combined *JHK* photometry on the CIT system (Elias et al. 1982) for the 40 objects presented in this paper. Column 1 gives the abbreviated object name, column 2 the adopted spectral type, and column 3 references for the spectral types, including the discovery reference. For L dwarfs we have adopted spectral types based on the optical spectrum classification system of Kirkpatrick et al. (2000), supplemented by work from several other authors, while for T dwarfs we have adopted spectral types based on the infrared spectrum classification system of Burgasser et al. (2002a), supplemented by the system of Geballe et al. (2002). The three exceptions to this are for the three L dwarfs SDSS J003259+1410, SDSS J010752+0041, and SDSS J144600+0024, for which no optical classifications have been published. For SDSS J083008+4828, we use an unpublished optical classification from Kirkpatrick et al. (2004). We note that these choices leave a gap between L8 and T0 as there are, so far, no L dwarfs later than L8 so far classified in the Kirkpatrick et al. (2000) system. See §15 for further discussion of spectral types for several objects of special interest.

The *JHK* photometry given in columns 4 through 6 is combined from several sources: the 2MASS All-Sky PSC (www.ipac.caltech.edu/2mass) transformed to the CIT system by the relations of Carpenter (2001), for L-dwarfs MKO photometry (Leggett et al. 2002) transformed to CIT by the relations of Hawarden et al. (2001), previously published USNO photometry (D02) which is on the CIT system (Guetter et al. 2003), UKIRT photometry for four objects (Leggett et al. 2000) transformed to the CIT system by the relations of Hawarden et al. (2001), and the small amount of new USNO CIT system photometry presented in Table 5. The listed photometric values are weighted mean values based on the published photometric errors after transformation to the CIT system. Column 7 gives references to the photometry employed.

For the purposes of this paper we have chosen to employ published empirical transformations from the various systems to the CIT system. Stephens and Leggett (2004) have pointed out the potential dangers in using transformations based on normal stars for L and T dwarfs and have calculated synthetic transformations from various systems to the MKO system. Examination of their results show that the predicted systematic errors are only a few percent for all transformations,

except for the 2MASS to CIT transformation at K band which are approximately 0.05 mag for L dwarfs and ranging from 0.10 mag for early and mid T dwarfs to as large as 0.20 mag for the latest T dwarfs. However, 2MASS photometry for the late T dwarfs studied here is either unavailable or with intrinsic photometric errors at the 0.2 mag level. Thus, random errors, along with the reported 0.05 to 0.25 mag intrinsic variations for these objects (Enoch, Brown, & Burgasser 2003) dominate this potential source of systematic error.

14. Discussion

In this section we present selected infrared absolute magnitude versus spectral type and infrared color relationships. At the risk of being accused of astronomical chauvinism, we have chosen for the remainder of this paper to discuss only USNO–derived optical and infrared parallaxes (this paper and D02). This provides a self–consistent set of parallax and proper motion determinations using the same telescope and similar observing philosophies and reduction software, with only the detector being different. When we publish completed parallax solutions, it will then be appropriate to combine these results with those of other researchers. Four of the objects, 2MASS J085035+1057AB, 2MASS J122554–2739AB, 2MASS J172811+3948AB, and 2MASS J210115+1736AB are known binaries. We discuss how the separated spectral types and photometry are determined in §15.4, §15.6, §15.8, and §15.9, respectively.

14.1. Absolute Magnitude versus Spectral Type

In Figure 2 we plot J-band absolute magnitude (M_J) versus spectral type. The solid data points are the results from this paper, where we have combined the infrared parallaxes with the infrared photometry and spectral classifications listed in Table 6. The photometric errors have been convolved with the parallax uncertainties to produce the vertical error bars. The horizontal errors are ± 0.5 spectral type for those objects with well-determined spectral classification and ± 1.0 spectral type for those with less certain classifications. The open data points are from D02 where we have used the parallaxes, infrared photometry, and spectral types published in that paper. For the seven objects in common between D02 and this paper, we plot both the CCD- and infrared-derived absolute magnitudes using the photometry of Table 6. In order to be consistent photometrically, we plot T513–46546 (D02) using 2MASS All-Sky PSC photometry transformed to CIT values by the Carpenter (2001) transformations. Several of the objects, in both the infrared and optical parallax groups, are known binaries and we have plotted them in accordance with what is known about their binary natures. These objects are discussed individually in § 15 and § 16 below. In Figures 3 and 4 we plot the M_H and M_K absolute magnitudes, respectively, versus spectral type with the same considerations as for Figure 2.

Our results for spectral types earlier than about L5 do not provide much new information,

since we have only a few early L dwarfs, some of which currently have large error bars. However, the results are consistent with narrow loci in all three diagrams. For objects between L5 and L9 the dispersion is clearly much greater than for earlier objects. The widths are about 1.5 mag, 1.3 mag, and 1.0 mag in J, H, and K, respectively, for the L5–8 objects. While this could be due to an admixture of objects of different ages, masses, and gravities, we have looked, within a given spectral type, for correlations of M_J , M_H , and M_K with tangential velocities (see §14.3) as a potential age indicator, but have found none. More likely, the additional width is due to the complicated atmospheric physics expected for late L dwarfs (Burgasser et al. 2002b; Stephens 2003), which also can explain why the spread is a function of wavelength. These models also predict significant variability due to rapid evolution or motion of cloud holes, which alone could be responsible for the apparent spread in absolute magnitude. Clearly photometric monitoring will be necessary to fully understand the L–T transition objects.

In all three diagrams the transition from L to T dwarfs is smooth. The excess in luminosity for T1–5 spectral types, previously noted by D02 and TBK03, is clearly substantiated by our enhanced database. While this excess is most evident in the J band, it is also seen in the H and K bands. The possibility that the early T dwarf luminosity excess is caused by contamination due to binary systems (Burgasser 2001) now seems unlikely due to the sheer number of objects which participate in this hump. TBK03 point out that the amplitude of the hump, like the spread at late L, is also unlikely to be explained by an age selection effect (Tsuji & Nakajima 2003). T dwarfs between T6 and T8 once again form a rather tight locus terminating at $M_{J,H,K} \approx 16.6$.

The additional data for T dwarfs allow a somewhat clearer picture of the L–T transition region in these diagrams. While there is no self-evident reason to believe that M_J , M_H , or M_K should map linearly with spectral type (TBK03), we note that inspection of Figures 2 through 4 shows that the late T dwarfs (T6–T8) are on a rough extension of the absolute magnitude versus spectral type relation of the the early L dwarfs (L0–L5). Relative to a fiducial line drawn between the early Ls and late Ts, in J–band the L–T transition objects show a luminosity deficit of about 1.5 mag at L6–L8 and a luminosity excess of about 1.5 mag at T1–T5. In H–band the L6–L8 deficit has shrunk to about 0.5 mag and disappears at K–band, while in H– and K–bands the excess for T1–T5 objects remains at 1.0–1.5 mag.

We note that the contrast between the large spread of absolute magnitudes at late L versus the apparently narrow locus of early T absolute magnitudes may not be significant. The narrow T dwarf locus may yet prove to be an artifact of small number statistics. Also, spectral typing may just map out an equivalent diversity of physics over a smaller range of spectral types at late L than at early T.

14.2. Absolute Magnitude versus Infrared Colors

In Figure 5 we plot M_J versus $J - H$ color. The solid data points are the results from this paper, where we have combined the infrared parallaxes with the infrared photometry and spectral classifications listed in Table 6. The photometric errors have been convolved with the parallax uncertainties to produce the vertical error bars, while the horizontal errors are from Table 6. The open data points are those from D02, where we have used the parallaxes, infrared photometry, and spectral types published in that paper. We treat the seven objects in common between D02 and this paper and the binary systems as described in §14.1. In Figure 6 we plot M_J versus $J - K$ color, while in Figures 7 and 8 we plot M_K versus $J - H$ and $J - K$, respectively.

These figures show the well-known color trends for L dwarfs ranging from $J - H \approx 0.7$, $J - K \approx 1.1$ for L0 ($M_J \approx 11.0$, $M_K \approx 10.0$) to $J - H \approx 1.2$, $J - K \approx 2.1$ for L8 ($M_J \approx 15.0$, $M_K \approx 13.5$). Late T dwarfs (T5 to T8) all have roughly $J - H \approx 0$, $J - K \approx 0$, while early T dwarfs (T0.5 to T4.5) have a wide range of colors transitioning between late L and late T colors. Several objects are now placed in the transition region between the loci of the L and T dwarfs, which is best shown in the M_K versus $J - K$ diagram (Figure 8). Unfortunately, the locations of many of the transition objects and early T dwarfs are poorly known at this time due to uncertain distances. We will defer comparing evolutionary models with observations until we obtain final parallaxes and further USNO-CIT photometry. However, we note that the apparent brightening in M_J across the L–T transition is consistent with the predictions of the cloud hole model of Burgasser et al. (2002b), while the fact that the brightening is an apparent trend argues against the hypothesis of Tsuji & Nakajima (2003) that it is simply an age effect.

14.3. Kinematics

For stars in the solar vicinity, motion with respect to the Sun is an indicator of age, since older stars will have had time to be perturbed preferentially to different orbits by interaction with the Galactic disk. Because T dwarfs are thought to be the cooler and older analogs of at least some L dwarfs, it might be expected that T dwarfs will have a larger mean velocity, with respect to the Sun, than L dwarfs. The measured tangential velocities (V_{tan}) with respect to the Sun measured primarily for L dwarfs in D02 can be combined with those for L and T dwarfs in this paper (Table 2) to have sufficient objects in order to compare the velocity distributions. For the seven objects in common between the two papers we use the weighted mean values of V_{tan} . We remove three objects from consideration with exceptionally large V_{tan} uncertainties, having both $\sigma(V_{tan}) > 10 \text{ km s}^{-1}$ and $V_{tan}/\sigma(V_{tan}) < 3$ (two L dwarfs: 2MASS J143535–0043 [$31.7 \pm 13.3 \text{ km s}^{-1}$] and 2MASS J095105+3558 [$55.8 \pm 32.7 \text{ km s}^{-1}$] and one T dwarf: SDSS J083717–0000 [$24.3 \pm 11.8 \text{ km s}^{-1}$]; all from this paper). This leaves 33 L dwarfs and 17 T dwarfs to make the velocity comparison. The unweighted average values of tangential velocity for L and T dwarfs, respectively, is 30.0 ± 3.6 and $43.0 \pm 4.8 \text{ km s}^{-1}$. The median values are, for L and T dwarfs respectively, 24.5 and 39.0 km s^{-1} .

As D02 have discussed, the velocity of the L dwarfs is consistent with velocities for old disk M and dM stars.

The distributions of V_{tan} are shown in Figure 9 for L dwarfs in the top panel and for T dwarfs in the bottom panel. Based on the Kolmogorov–Smirnov test, the null hypothesis that the two distributions are indistinguishable can only be rejected at the 73% level. The main difference is that the T dwarfs have no examples with $V_{tan} \leq 20 \text{ km s}^{-1}$, whereas the L dwarfs have 11 of 33 (33%) with $V_{tan} \leq 20 \text{ km s}^{-1}$. While there are fewer objects in the T dwarf subset, if the distributions were the same, 5.7 T dwarfs with $V_{tan} \leq 20 \text{ km s}^{-1}$ would be expected.

15. Discussion of Individual Objects

There are several objects which, after our new parallax results, warrant special attention. We discuss these briefly here.

15.1. 2MASS J041519–0935

This object is the assigned T8 standard on the Burgasser et al. (2002a) classification system, which we have adopted as the primary classification system for T dwarfs in this paper. However, in the classification system of Geballe (2002) it is T9 (Knapp et al. 2004), indicating that it is likely the latest spectral type T dwarf yet found. Although it makes little quantitative difference, we plot and fit the the object as a T8.5, to recognize its extremely late spectral type. With a parallax of $174.3 \pm 2.8 \text{ mas}$ ($5.74 \pm 0.09 \text{ pc}$) it is one of the closest known brown dwarfs. Combining this distance with its 2MASS photometry gives it the lowest absolute magnitude of any T dwarf known: $M_J = 16.92 \pm 0.07$ (see §17). We estimate a bolometric magnitude of $M_{bol} = 18.70 \pm .26$, a luminosity of $\log(L/L_{\odot}) = -5.58 \pm 0.10$, and, hence, a temperature of $T_{\text{eff}} = 760 \pm 80 \text{ K}$, making it the least luminous and coldest brown dwarf yet discovered. See §18 for our discussion of bolometric corrections and temperature estimates for T dwarfs.

15.2. SDSS J042348–0414

The L–T transition object SDSS J042348–0414 has unusual spectral properties such that in the near–infrared Geballe et al. (2002) classify it as a T0, while in the optical Cruz et al. (2003) and Kirkpatrick et al. (2004) classify it as an L7.5. Both classifications are correct in the wavelength regions considered. It has a K–band bolometric correction which is typical of L7.5 to T0 objects (Golimowski et al. 2004). At L7.5 it lies at the top of the loci for late L dwarfs in the spectral type versus absolute magnitude diagrams of Figures 2 through 4, about a factor of two brighter than the average for late L dwarfs. At T0 it lies well above the locus for early T dwarfs in these same

diagrams; about a factor of 4 brighter than the average for early T dwarfs. While this could be explained by binarity (multiplicity in the case of T0), no HST observations have yet been obtained to help resolve this issue. While we have not yet carried out a formal search for perturbations, there is no evidence in the astrometric data to indicate either perturbations or difficulty in centroiding for this nearby (15.2 pc) object. From §11, for the group of 22 objects with average $\Delta t = 2.03$ yr, the mean parallax error is 3.86 mas and the mean proper motion error is 5.20 mas yr^{-1} . SDSS J042348–0414 has $\Delta t = 2.02$ yr, with mean parallax and proper motion errors of 1.70 mas and 2.80 mas yr^{-1} , respectively. Another possibility is that this object is still very young and thus over-luminous due to a radius larger than for older brown dwarfs. For the purposes of this paper we will use the L7.5 classification since it lies within the absolute magnitude loci of late L dwarfs and its near-infrared colors are not inconsistent with this spectral classification. Clearly further investigation will be needed to understand the nature of this enigmatic object.

15.3. 2MASS J055919–1404

2MASS J055919–1404 has historically been considered enigmatic since it appeared to have an absolute magnitude considerably larger than objects of similar spectral type. Although it has been suspected of being an equal mass binary (Burgasser 2001; D02), recent Hubble Space Telescope Wide Field/Planetary Camera 2 (WFPC2) observations have failed to reveal a bright binary companion at a separation larger than 0.05 arcsec (Burgasser et al. 2003a), although such a system could currently be hidden in an unfavorable orientation. Our data adds considerably to the census of T1–5 objects which populate the hump seen in the spectral type versus absolute magnitude diagrams (Figures 2–4). These results indicate that 2MASS J055919–1404 lies at least much closer to the loci of other objects in this spectral range than was previously thought. It will require further luminosity determinations of other T1–5 objects and other observations of 2MASS J055919–1404 itself to determine whether this object is indeed overluminous or simply the prototype hump object lying at the peak of this local luminosity maximum.

15.4. 2MASS J085035+1057AB

2MASS J085035+1057AB was found by Reid et al. (2001) to be a binary system with a separation of 0.16 arcsec from HST WFPC2 observations. Based on optical colors from these observations they estimate a J-band magnitude difference of $\Delta M = 0.9$. Adopting this magnitude difference, the photometry listed in Table 6, and our parallactic distance we find a value of $M_J = 13.78$ for the A component, which is consistent with the L6V spectral type for the dominant component found by Kirkpatrick et al. (1999, see Figure 2). The B component has $M_J = 14.68$, which is consistent with a late-L, early-T, or a T6 spectral type (again see Figure 2). A mid to late T spectral type can probably be ruled out on the basis of the combined spectrum (Reid et al. 2001). Since late-L dwarf colors range between $(J - K) \approx 1.6$ –2.0 and early-T colors cluster around $(J - K) \approx 1.0$,

measurement of a K magnitude alone would likely distinguish between a late-L and early-T spectral type for the B component.

15.5. 2MASS J093734+2931

The second faintest T dwarf in our sample, and one of the closest (6.14 ± 0.15 pc), is 2MASS 093734+2931, which was classified as a peculiar T6 by Burgasser et al. (2002) due to its extremely blue near-infrared color ($(J - K) = -0.72 \pm 0.20$; Table 6). This object is indeed peculiar, in that it is over 3 times less luminous and about 300 K cooler than the typical T6 dwarf observed (see §18 and §19). Burgasser et al. (2002, 2003b) postulate that 2MASS 093734+2931 may be a metal-poor and/or high gravity (i.e. old and massive) brown dwarf based on the enhanced collisionally-induced H₂ absorption that gives it its blue near-infrared colors. These gravity/metallicity effects may be substantial enough to modify the near-infrared spectrum so that it appears to be an earlier-type (hotter) brown dwarf than its true T_{eff} . Alternatively, K-band bolometric corrections for this object may also be biased, due to the substantial suppression of flux at these wavelengths (Golimowski et al. 2004). However, given that this object is subluminescent in all near-infrared bands as compared to other T6 dwarfs, metallicity and/or gravity differences are clearly important in these cool brown dwarfs and must be quantified before a universal spectral type/temperature relation can be derived.

15.6. 2MASS J122554–2739AB

2MASS J122554–2739 is a clearly separated double system with an angular separation of 0.282 ± 0.005 arcsec from HST WFPC2 observations (Burgasser et al. 2003a). Based on optical colors from these observations they speculate that the system is composed of T6V and T8V components and estimate a J-band magnitude difference of $\Delta M_J = 1.35 \pm 0.08$. Adopting this magnitude difference and assuming that it also applies to H- and K-band (since late T dwarf *JHK* colors scatter around 0.0), we use the available 2MASS photometry transformed to the CIT system, and apply our parallactic distance determination to produce the *JHK* absolute magnitudes listed in Table 7 (see §17) and plotted in Figures 2 through 8. The infrared absolute magnitudes are consistent with T6V and T8V for components A and B, respectively.

Our parallax result increases the projected separation of the components to 3.80 ± 0.18 AU, from the 3.18 AU separation based on the spectrophotometric distance (Burgasser et al. 2003a). This, in turn, increases the estimated orbital period of the system to between 31 and 53 years, based on the effective temperatures and age range assumed by Burgasser et al. (2003a), but does not alter their conclusion that direct orbital motion of this system could be detected over a short time range.

15.7. SDSS J143517–0046 and SDSS J143535–0043

SDSS J143517–0046 and SDSS J143535–0043 were put on the infrared parallax program partially because, at an angular separation of about 5 arcmin, they could be a common proper motion pair. While the current parallax results do not rule out the possibility that they are at the same distance, the proper motions are nearly a factor of four different in magnitude and the position angles nearly orthogonal. Thus, the angular proximity of these objects appears to be fortuitous.

15.8. 2MASS J172811+3948AB

Gizis et al. (2003) found this to be a binary with 0.13 arcsec separation using the HST WFPC2 camera. They found the A component to be 0.3 mag brighter than the B component in I band, but 0.3 mag fainter in Z band, which they interpret as the B component being an L/T transition object. Since the $J - H$ and $J - K$ colors (Table 6) are normal for the L7 spectral classification (Kirkpatrick et al. 2000) and absolute JHK magnitudes are approximately equal for late L to early T, we assume that the flux is evenly split between the two components in the infrared to produce the JHK absolute magnitudes listed in Table 7 (see §17) and plotted in Figures 2 through 8.

15.9. 2MASS J210115+1756AB

Gizis et al. (2003) found this to be a binary with 0.232 arcsec separation using the HST WFPC2 camera. They find the B component to be slightly later than the L7.5 classification of the system (Kirkpatrick et al. 2000). Since the colors and absolute JHK magnitudes are similar for late L dwarfs, we assume that the flux is evenly split between the two components in the infrared to produce the JHK absolute magnitudes listed in Table 7 (see §17) and plotted in Figures 2 through 8.

16. Binaries in the CCD Dataset

There are four additional binary systems in the CCD astrometry set which we treat in a manner similar to that of D02. Two systems have components of equal near-infrared magnitudes: DENIS 020529–1159AB (Koerner et al. 1999; Leggett et al. 2001) and DENIS 122815–1547AB (Koerner et al. 1999). For these systems we assume that the components have identical spectral types and plot the absolute magnitudes with the assumption that the flux is split evenly between the components.

In the case of 2MASS J074642+2000AB, Reid et al. (2001) estimate a J-band magnitude difference of $\Delta M_J = 0.47$ based on optical colors from HST WFPC2 observations. We use this magnitude difference to estimate the J magnitude for the L0.5 primary component and assume

that the combined light colors apply to the primary to estimate its H and K magnitudes. While there is not enough information available to uniquely determine the nature of the B component, we note that its resultant $M_J = 12.31 \pm 0.02$ is consistent with its being about an L3V. Since JHK colors of L0.5 and L3 objects are similar (Table 9), our assumption that the system JHK colors are applicable to the primary for determining M_H and M_K is reasonable.

For 2MASS J114634+2230AB, Reid et al. (2001) estimate a J-band magnitude difference of $\Delta M = 0.23$, again based on optical colors from HST WFPC2 observations and we again use this magnitude difference to correct the J magnitude for the L3 primary component and assume that the combined light JHK colors apply to the primary. The small difference in ΔM indicates that the B component must be near an L3 also and that our assumption that the system JHK colors are applicable to the primary for determining M_H and M_K is reasonable.

17. Absolute JHK Magnitudes Based on Optical and Infrared Parallaxes

In this section we combine the adopted spectral types and CIT system photometry from Table 6 with the infrared parallaxes presented in this paper (Table 2) and the optical parallaxes derived by D02 to derive CIT system absolute magnitudes M_J , M_H , and M_K . These are presented in Table 7 in order of spectral type. We note that the spectral types used for the objects in D02 conform to the convention for L and T spectral types described in §13. In the seven cases where both USNO optical and infrared parallaxes are available, we combined the parallaxes, weighting by the listed uncertainties. The first three columns give the abbreviated object names, adopted spectral type, and whether optical, infrared, or combined parallaxes were used, respectively. The last six columns give M_J , M_H , and M_K and their uncertainties, respectively. We have not included the B components of binaries where spectral types are uncertain.

For the 36 objects from L0 to L8 (excluding the enigmatic object SDSS J042348–0414) we use the data of Table 7 to derive the following equations giving the best linear fits of M_J , M_H , and M_K , respectively, with spectral type (ST), where we numerically encode $ST_L = 0$ for L0, $ST_L = 5$ for L5, etc. There is no evidence for significant second order terms for any of the bandpasses. We weighted the data by the inverse square of the larger of the $\sigma(-)\sigma(+)$ values and, since these are all ‘preliminary’ parallaxes degraded the minimum error to 0.05 mag such that the few objects with very small formal errors would not dominate the fits. The uncertainties listed at the end of each equation show the dispersions from the fits, in magnitudes.

$$M_J = 11.62 + 0.380 \times (ST_L), \sigma = 0.24 \quad (1)$$

$$M_H = 10.85 + 0.346 \times (ST_L), \sigma = 0.19 \quad (2)$$

$$M_K = 10.33 + 0.324 \times (ST_L), \sigma = 0.17 \quad (3)$$

The changing slopes with bandpass reflect the fact that the L dwarfs become redder with later spectral type. Our results are consistent with those of D02 who report an M_J slope of 0.347 and

scatter of $\sigma = 0.24$ mag for objects between M6.5V and L8.

For the 19 T dwarfs between T0.5 and T8 the following quadratic equations adequately describe the M_J , M_H , and M_K versus spectral relations where $ST_T = 0$ for T0, $ST_T = 5$ for T5, etc. In this case we have degraded the minimum uncertainty to 0.10 mag so that essentially one object would not dominate the fit.

$$M_J = 15.04 - 0.533 \times (ST_T) + 0.091 \times (ST_T)^2, \sigma = 0.36 \quad (4)$$

$$M_H = 13.66 - 0.139 \times (ST_T) + 0.063 \times (ST_T)^2, \sigma = 0.44 \quad (5)$$

$$M_K = 13.22 - 0.055 \times (ST_T) + 0.060 \times (ST_T)^2, \sigma = 0.62 \quad (6)$$

18. L and T Dwarf Luminosities and Effective Temperature Estimates

L and T dwarf luminosities and effective temperatures can be estimated for objects with known distances. D02 have previously made such estimates for mid-M stars through late L dwarfs, but this has been difficult to do for T dwarfs due to the paucity of bolometric corrections ($BC_{filt} = M_{bol} - M_{filt}$) which have previously been measured for these objects (e.g. for 2MASS J055919–1404 [Burgasser 2001]; for Gliese 229B [Leggett et al. 1999; Leggett et al. 2002]; for Gliese 570D [Burgasser et al. 2000; Geballe et al. 2001; Leggett et al. 2002]). However, Golimowski et al. (2004) have recently calculated BC_K for a large number of both L and T dwarfs, greatly expanding the number of consistently-derived bolometric corrections available for these objects. Moreover, they have included L' and M' photometry in their BC calculations, such that most of the spectral energy distributions of L and T dwarfs are now covered for the first time, allowing more reliable estimates of bolometric corrections and, hence, bolometric magnitudes to be made.

We use the M_K values from Table 7 and apply the fourth order polynomial fit of BC_K versus spectral type from Table 4 of Golimowski et al. (2004) to determine M_{bol} for L and T dwarfs which have USNO parallaxes. The resultant M_{bol} values, along with their balanced uncertainties, are listed in column 3 of Table 8. We note that the M_K values are on the CIT system, while the Golimowski et al. (2004) BC_K determinations are formally for the K_{MKO} filter. However, the synthetic transformations of Stephens and Leggett (2004) show that the CIT and MKO filters give nearly identical results for L and T dwarfs, with offsets of 0.01-0.02 mag for L0 to L8 and 0.02-0.09 mag for T0.5 to T8. These small offsets are dominated by other sources of uncertainty but are added to the error budget. Also the Golimowski et al. (2004) BC_K versus spectral type calibration is for the spectral classification system of Geballe et al. (2002), which includes L and T spectral types as late as L9 and T9, but we expect no significant effects from this. The errors listed for M_{bol} are the quadrature sums of the following uncertainties: $0.02 \leq \sigma(M_K) \leq 1.28$ mag, $0.01 \leq \sigma(K_{CIT} - K_{MKO}) \leq 0.09$ mag, and $\sigma(BC) = 0.13$ mag. Assuming for the Sun $M_{bol} = +4.74$ (Drilling & Landolt 2000), we list the derived logarithmic luminosities in units of solar luminosity along with their uncertainties in column 4 of Table 8.

Effective temperatures (T_{eff}) for L and T dwarfs can be estimated from $L = 4\pi R^2 \sigma T_{\text{eff}}^4$, normalized to solar units, by

$$M_{\text{bol}} = 42.36 - 5 \log(R/R_{\odot}) - 10 \log T_{\text{eff}} \quad (7)$$

(Drilling & Landolt 2000). L and T dwarf radii are largely, but not totally, independent of mass and age, with a range of about 30%. Burgasser (2001) performed a Monte Carlo analysis of the Burrows et al. (1997) L and T dwarf evolutionary models, to understand the distribution of radii for objects between 0.001 and 10 Gyr in age and masses between 1.0 and 100 M_{JUP} . The mean radius for the model assuming constant birth rate and the mass function $dN \propto M^{-1} dM$ is 0.90 R_{JUP} . A total radius range of about 0.75 to 1.05 R_{JUP} results from these simulations. We use a radius of $0.90 \pm 0.15 R_{\text{JUP}}$ and the previously derived values of M_{bol} and its uncertainties to derive the T_{eff} values and their range which are listed in the last column of Table 8. At $\log(L/L_{\odot}) = -5.58 \pm 0.10$ and $T_{\text{eff}} \approx 760$ K, 2MASS J041519–0935 is found to be the coldest and least luminous brown dwarf yet discovered.

While luminosities and temperatures drop quickly with spectral type for early L and late T objects, the derived values of M_{bol} and $\log(L/L_{\odot})$ show only a small range between about L6 to T5. When combined with the assumptions about brown dwarf radii above, this implies a temperature range of only about 1200 to 1550 K. A similar narrow range in T_{eff} was predicted by Kirkpatrick et al. (2000) based on luminosity estimates for Gliese 584C (L8) and Gliese 229B (T6.5). Such a narrow T_{eff} range over a substantial shift in spectral morphology is predicted by Burgasser et al. (2000b), who postulate that the L–T transition is dominated by condensate cloud evolution, rather than cooling. However, more recent cloud models (e.g. Tsuji & Nakajima 2003) also predict a rapid evolution from L to T without the need for atmospheric dynamics. Clearly, synoptic monitoring, over a range of timescales, both photometrically and spectroscopically, will need to be a high priority in order to understand better the competition between cloud condensation and turbulent cloud disruption in these objects.

We note that our derived temperatures for the earliest L dwarfs of about 2400-2500 K are warmer by about 200-300 K than some earlier estimates (e.g. Leggett et al. 2001,2002) but consistent with those derived by D02. We again direct attention to Golimowski et al. (2004), not only for their definitive BC calculations, but also for determinations of luminosities and temperatures for a somewhat different sample of objects, using a different photometric database and slightly different assumptions about brown dwarf radii.

19. Mean Derived Properties of L and T Dwarfs

In Table 9 we present mean derived properties of brown dwarfs based on the work of this paper. The spectral type ranges listed in column 1 (L0 to L8 and T0.5 to T8) span those of objects with USNO optical or infrared parallaxes. M_J , M_H , and M_K listed in columns 2, 3, 4, respectively, are calculated from equations (1) through (6) of §17, while the $J - H$ and $J - K$ colors in columns

5 and 6, respectively, are differences from these equations. M_{bol} , $\log(L/L_{\odot})$, and T_{eff} in columns 7, 8, and 9, respectively, are derived from the listed M_K values and the methods discussed in §18. T_{eff} values are rounded to the nearest 10 K. We caution that the values in Table 9 should be treated as schematic results only, as they do not represent the full width and subtle variations in the spectral type versus absolute magnitude relations of Figures 2 through 4. With better astrometry, photometry, and knowledge of brown dwarf variability some of the apparent details in these figures may prove to be false, while others may prove to represent stellar and sub-stellar physics.

20. Future Work

As with the USNO optical parallax and proper motion program, it is our intent that the infrared astrometry program will be a long-term enterprise. All of the objects listed in this paper will be observed for a minimum of three years, to ensure a full distribution of observations over the parallactic ellipse, before final astrometric results are reported. Fainter objects and/or those with poorer reference frames will need a longer period of time. Our goal will be to provide 1.0 mas or better parallaxes for as many objects as possible, although it may not be a feasible goal for all objects. Objects with special astrophysical significance may be left on the program longer to achieve even higher precision.

It can be anticipated that many more brown dwarfs will be found by further mining of large-sky databases. As objects are removed from the current program as they are completed, new objects will be added to the program when they can fit into a depleted right ascension slot. We have already expanded our program from the initial 40 objects to 52 objects. Most of the new objects are T dwarfs as we wish to utilize our resources on objects that are observed to advantage in the infrared while problematic for the optical CCD program. From experience with our current observing mode, a program consisting of 50 to 60 objects is a practical limit. We intend to publish an update to our results about every two years, providing lists both of completed astrometry and preliminary results for new objects and objects with continuing observations.

A comparison of uncertainties listed in Table 6 and Table 7 shows that for several objects the uncertainty in absolute magnitude is largely due to uncertainty in infrared photometry. We intend to provide high quality USNO-CIT photometry, as in D02, for all objects for which we publish completed astrometry. These frames, along with the potential to obtain SDSS optical photometry from Flagstaff, will assure that photometric parallaxes of all suitable reference frame stars will be available to form the best possible relative to absolute parallax corrections.

An interesting related issue is the question of how much of the spread in brown dwarf loci in the spectral type and color versus magnitude diagrams is due, not to mean intrinsic brightness dispersion, but to variability, especially for the L–T transition objects. The results of a several night photometric monitoring campaign during one month (Enoch, Brown, & Burgasser 2003) show variability for 9 L and T dwarfs of 5–25% in K_s band. Our astrometric database should prove

to be valuable for investigation of J band variability of T dwarfs and H band variability of L dwarfs on time scales of minutes (one night’s data), days (one run’s data), months (one year’s data), and years (an entire astrometry dataset).

21. Summary

In this paper we have presented preliminary parallaxes and proper motions for 22 L dwarfs and 18 T dwarfs derived over time baselines of only $\Delta t \approx 1.3$ or $\Delta t \approx 2.0$ years. The resultant mean parallax uncertainties of 4.86 and 3.85 mas, respectively, which will be greatly improved by ongoing further observations, are nonetheless of sufficient quality to provide some significant new results for T dwarfs. We list here a summary of the more important conclusions we reach from our work.

A. The luminosity excess ‘hump’ for early to mid T dwarfs in the absolute magnitude versus spectral type diagram is clearly confirmed. While seen most strongly at J–band, it is also evident in the H– and K–bands. The possibility that the hump is due to a selection effect of binaries is likely ruled out by the large number of objects participating in the hump.

B. L5–L8 dwarfs have a significantly larger spread in the absolute magnitude versus spectral type diagrams than do earlier L dwarfs.

C. Late T dwarfs have a narrow locus in absolute magnitude versus spectral type diagrams, similar to the early L dwarfs. Relative to a straight line connecting the earlier and later objects, the L–T transition objects show systematic trends. In J–band the late L dwarfs show a luminosity deficit and the early T dwarfs a luminosity excess. The late L dwarf luminosity deficit is less in H–band and is gone in K band, while the early T dwarf luminosity excess amplitude is somewhat less in H–band and K–band than at J–band.

D. The absolute magnitude behavior across the L–T transition described above exemplifies the critical role of condensate cloud evolution at these temperatures based on the most recent spectral models.

E. Using newly derived bolometric corrections for L and T dwarfs by Golimowski et al. (2004) we derive luminosities and T_{eff} for L and T dwarfs with USNO–derived parallaxes either from this paper or D02.

F. 2MASS J041519–0935 is found to be the least luminous [$\log(L/L_{\odot}) = -5.58$] and therefore coldest ($T_{\text{eff}} \approx 760$ K) brown dwarf yet found.

G. We find a broader distribution of L dwarf tangential velocities compared with that of the T dwarfs. While essentially the same between 20 to 60 km s^{–1}, the T dwarfs do not have a low velocity population as do the L dwarfs. This is consistent with T dwarfs being, in general, older than L dwarfs.

This research has made use of the NASA/ IPAC Infrared Science Archive, which is operated by the Jet Propulsion Laboratory, California Institute of Technology, under contract with the National Aeronautics and Space Administration.

Funding for the Sloan Digital Sky Survey (SDSS) has been provided by the Alfred P. Sloan Foundation, the Participating Institutions, the National Aeronautics and Space Administration, the National Science Foundation, the U.S. Department of Energy, the Japanese Monbukagakusho, and the Max Planck Society. The SDSS Web site is <http://www.sdss.org/>.

The SDSS is managed by the Astrophysical Research Consortium (ARC) for the Participating Institutions. The Participating Institutions are The University of Chicago, Fermilab, the Institute for Advanced Study, the Japan Participation Group, The Johns Hopkins University, Los Alamos National Laboratory, the Max-Planck-Institute for Astronomy (MPIA), the Max-Planck-Institute for Astrophysics (MPA), New Mexico State University, University of Pittsburgh, Princeton University, the United States Naval Observatory, and the University of Washington.

We thank C. Dahn, H. Harris, and D. Monet for many helpful science discussions. We thank A. Hoffmann and the team at RVS for working with us to build ALADDIN arrays, the design of which was partially funded for this work. We thank D. Toomey and his team at Mauna Kea Infrared and J. Fischer and the team at the Naval Research Laboratory for designing and fabricating our astrometric imager ASTROCAM. AJB acknowledges support provided by NASA through Hubble Fellowship grant HST-HF-01137.01 awarded by the Space Telescope Science Institute, which is operated by the Association of Universities for Research in Astronomy, Inc., under NASA contract NAS 5-26555.

REFERENCES

- Abazajian, K., et al. 2003, *AJ*, 126, 2081
- Basri, G. 2000, *ARA&A*, 38, 485
- Becklin, E. E. & Zuckerman, B. 1988, *Nature*, 336, 656
- Bessel, M. S. & Brett, J. M. 1988, *PASP*, 100, 1134
- Burgasser, A. J., et al. 1999, *ApJ*, 522, L65
- Burgasser, A. J., et al. 2000, *ApJ*, 531, L57
- Burgasser, A. J. 2001, Ph.D. Dissertation, California Institute of Technology
- Burgasser, A. J., et al. 2002a, *ApJ*, 564, 421
- Burgasser, A. J., Marley, M. S., Ackerman, A. S., Saumon, D., Lodders, K., Dahn, C. C., Harris, H. C., & Kirkpatrick, J. D. 2002b, *ApJ*, 571, L151

- Burgasser, A. J., Kirkpatrick, J. D., Reid, I. N., Brown, M. E., Miskey, C. L., & Gizis, J. E. 2003a, *ApJ*, 586, 512
- Burgasser, A. J., Kirkpatrick, J. D., Liebert, J., & Burrows, A. 2003b, *ApJ*, 594, 510
- Burrows, A., et al. 1997, *ApJ*, 491, 856
- Carpenter, J. M. 2001, *AJ*, 121, 2851
- Chabrier, G. & Baraffe, I. 2000, *ARA&A*, 38, 337
- Cruz, K. L., Reid, I. N., Liebert, J., Kirkpatrick, J. D., & Lowrance, P. J. 2003, *AJ*, 126, 2421
- Dahn, C. C. 1997, in *IAU Symp. No. 189, Fundamental Stellar Properties: The Interaction Between Observation and Theory*, eds. T. R. Bedding, A. J. Booth, & J. Davis (Dordrecht: IAU), 19
- Dahn, C. C., et al. 2002, *AJ*, 124, 1170 (D02)
- Delfosse, X. et al. 1997, *A&A*, 327, L25
- Drilling, J. S. & Landolt, A. U. 2000, in *Allen's Astrophysical Quantities, Fourth Edition*, ed. A. Cox (New York: Springer-Verlag), 382
- Elias, J. H., Frogel, J. A., Matthews, K., & Neugebauer, G. 1982, *AJ*, 87, 1029 (erratum 87, 1893)
- Enoch, M. L., Brown, M. E., & Burgasser, A. J. 2003, *AJ*, in press
- Epchtein, N. 1997, in *The Impact of Large Scale Near-IR Surveys*, ed. F. Garzon (Dordrecht: Kluwer), 15
- Fan, X. et al. 2000, *AJ*, 119, 928
- Fischer, J., et al. 2003, in *Proc. SPIE 4841, Instrument Design and Performance for Optical/Infrared Ground-based Telescopes*, eds. M. Iye & A. F. M. Moorwood (Bellingham: SPIE), 564
- Fowler, A. M., Gatley, I., McIntyre, P., Vrba, F. J., & Hoffman, A. 1996, in *Proc. SPIE 2816, Symposium on Infrared Detection for Remote Sensing: Physics, Materials, and Devices*, eds. R. E. Longshore & J. W. Baars (Bellingham: SPIE), 150
- Shimasaku, K., & Schneider, D. P. 1996, *AJ*, 111, 1748
- Geballe, T. R., Saumon, D., Leggett, S. K., Knapp, G. R., Marley, M. S., & Lodders, K. 2001, *ApJ*, 556, 373
- Geballe, T. R., et al. 2002, *ApJ*, 564, 466
- Gizis, J. E., Reid, I. N., Knapp, G. R., Liebert, J., Kirkpatrick, J. D., Koerner, D. W., & Burgasser, A. J. 2003, *AJ*, 125, 3302
- Golimowski, D. A., et al. 2004, *AJ*, submitted

- Guetter, H. H., Vrba, F. J., Henden, A. A., & Luginbuhl, C. B. 2003, *AJ*, 125, in press
- Hawarden, T. G., Leggett, S. K., Letawsky, M. B., Ballantyne, D. R., & Casali, M. M. 2001, *MNRAS*, 325, 563
- Hawley, S. L., et al. 2002, *AJ*, 123, 3409
- Kirkpatrick, J. D. et al. 1999. *ApJ*, 519, 802
- Kirkpatrick, J. D., et al. 2000, *AJ*, 120, 447
- Kirkpatrick, J. D., et al. 2004, in preparation
- Knapp, G. R., et al. 2004, *AJ*, submitted
- Koerner, D. W., Kirkpatrick, J. D., McElwain, M. W., & Bonaventura, A. J. 1999, *ApJ*, 526, L25
- Leggett, S. K., Toomey, D. W., Geballe, T. R., & Brown, R. H. 1999, *ApJ*, 517, L139
- Leggett, S. K. et al. 2000, *ApJ*, 536, L35
- Leggett, S. K., Allard, F., Geballe, T. R., Hauschildt, P. H., & Schweitzer, A. 2001, *ApJ*, 548, 908
- Leggett, S. K. et al. 2002, *ApJ*, 564, 452
- Luginbuhl, C. B., Henden, A. A., Vrba, F. J., & Guetter, H. H. 1998, in *Proc. SPIE 3354, Infrared Astronomical Instrumentation*, ed. A. Fowler (Bellingham: SPIE), 240
- Luyten, W. J. 1979, *NLTT Catalog* (University of Minnesota)
- Martín, E. L., Delfosse, X., Basri, G., Goldman, B., Forveille, T., & Zapatero-Osorio, M. R. 1999, *AJ*, 118, 2466
- Monet, D. G. & Dahn, C. C. 1983, *AJ*, 88, 1489
- Monet, D. G., Dahn, C. C., Vrba, F. J., Harris, H. C., Pier, J. R., Luginbuhl, C. B., & Ables, H. D. 1992, *AJ*, 103, 638
- Nakajima, T., Oppenheimer, B. R., Kulkarni, S. R., Golimowski, D. A., Matthews, K., Durrance, S. T. 1995, *Nature*, 378, 463
- Oppenheimer, B. R., Kulkarni, S. R., Matthews, K., & Nakajima, T. 1995, *Science*, 270, 1478
- Reid, I. N., Gizis, J. E., Kirkpatrick, J. D., & Koerner, D. W. 2001, *AJ*, 121, 489
- Schlegel, D. J., Finkbeiner, D. P., & Davis, M. 1998, *ApJ*, 500, 525
- Schmidt-Kaler, Th. 1982, *Landolt-Borstein, New Series, Group VI* (New York: Springer), Subvolume 2b, 453

- Schneider, D. P. et al. 2002, *AJ*, 123, 458
- Siegel, M. H., Majewski, S. R., Reid, I. N., & Thompson, I. B. 2002, *ApJ*, 578, 151
- Skrutskie, M. F. 1997, in *The Impact of Large-Scale Near-IR Sky Surveys*, ed. F. Garzon et al. (Dordrecht: Kluwer), 25
- Stephens, D. C. 2003, in *IAU Symp. 211, Brown Dwarfs*, ed. E. Martín (San Francisco; ASP), 355
- Stephens, D. C. & Leggett, S. K. 2004, *PASP*, 116, 9
- Stone, R. C. 1997, *AJ*, 114, 2811
- Strauss, M. A., et al. 1999, *ApJ*, 522, L61
- Tinney, C. G., Burgasser, A. J., & Kirkpatrick, J. D. 2003, *AJ*, 126, 975 (TBK03)
- Tsuji, T. & Nakajima, T 2003, *ApJ*, 585, L151
- Tsvetanov, Z. I. et al. 2000, *ApJ*, 531, L61
- Vrba, F. J., Henden, A. A., Luginbuhl, C. B., Guetter, H. H., & Monet, D. G. 2000, *BAAS*, 32, 678
- York, D. G., et al. 2000, *AJ*, 120, 1579

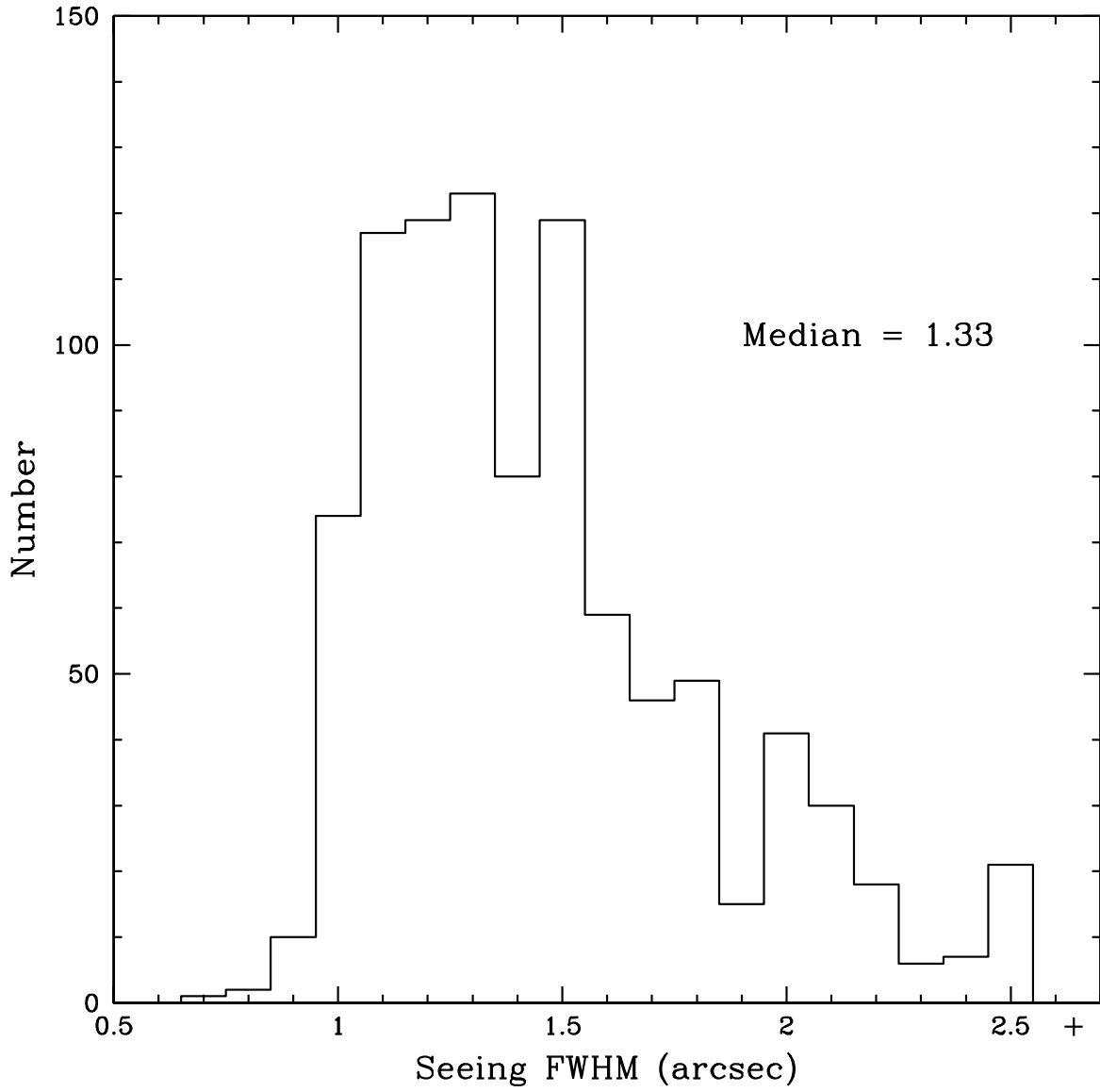


Fig. 1.— Histogram of the seeing (in the J and H bands) at the 1.55-m telescope using ASTROCAM at the beginning of each set of observations employed in this paper. The bar at 2.5+ arcsec represents those observations at 2.5 arcsec and slightly larger used in the solutions. The median seeing is 1.33 arcsec.

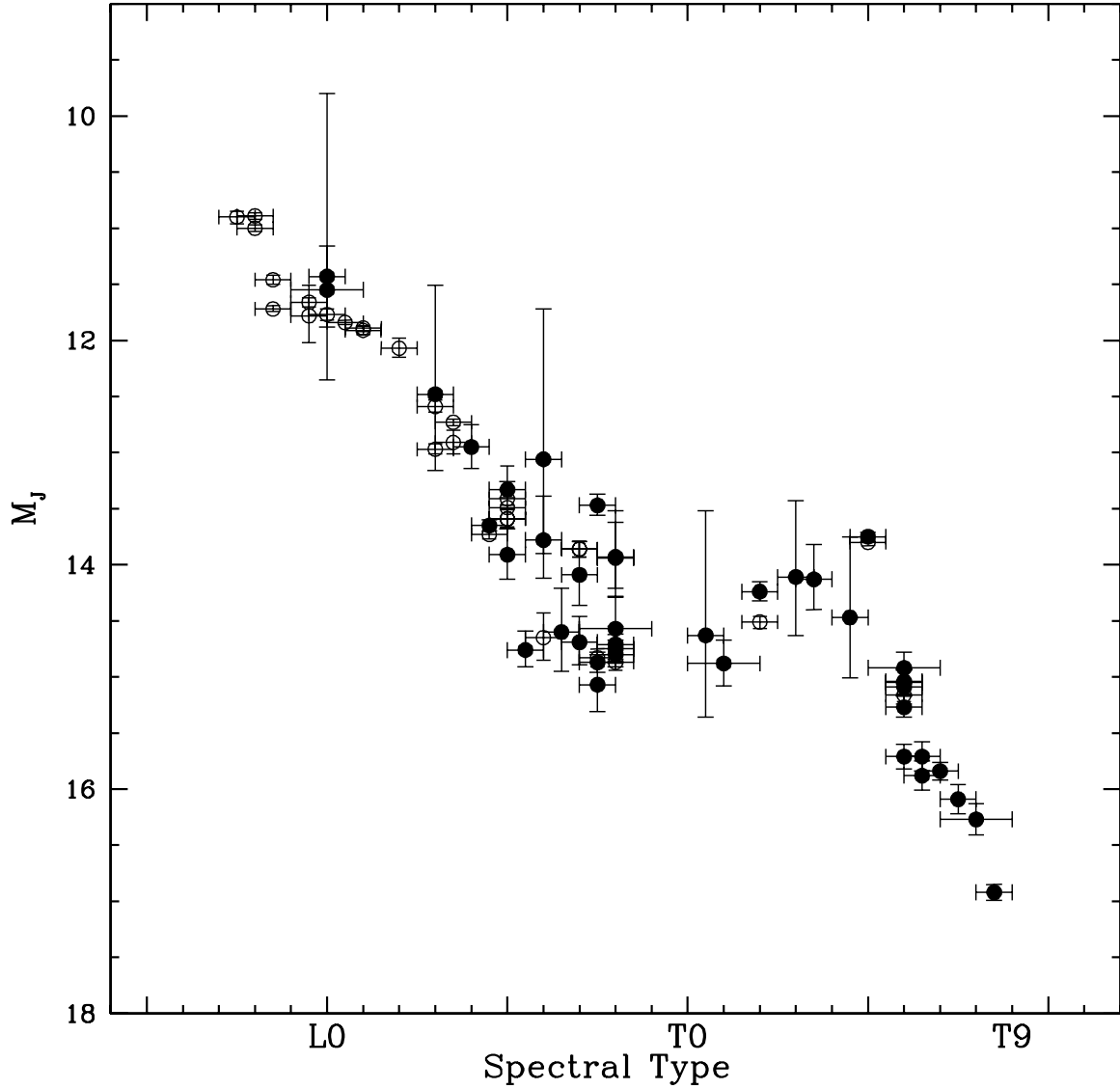


Fig. 2.— Absolute J-band magnitude (M_J) is plotted versus spectral type. The solid data points are the results from the infrared astrometry and photometry from Table 6 of this paper; the open points are the results of optical astrometry from D02. For the seven objects in common, results are plotted for both optical and infrared parallaxes. A complete description of this figure is given in §14.1.

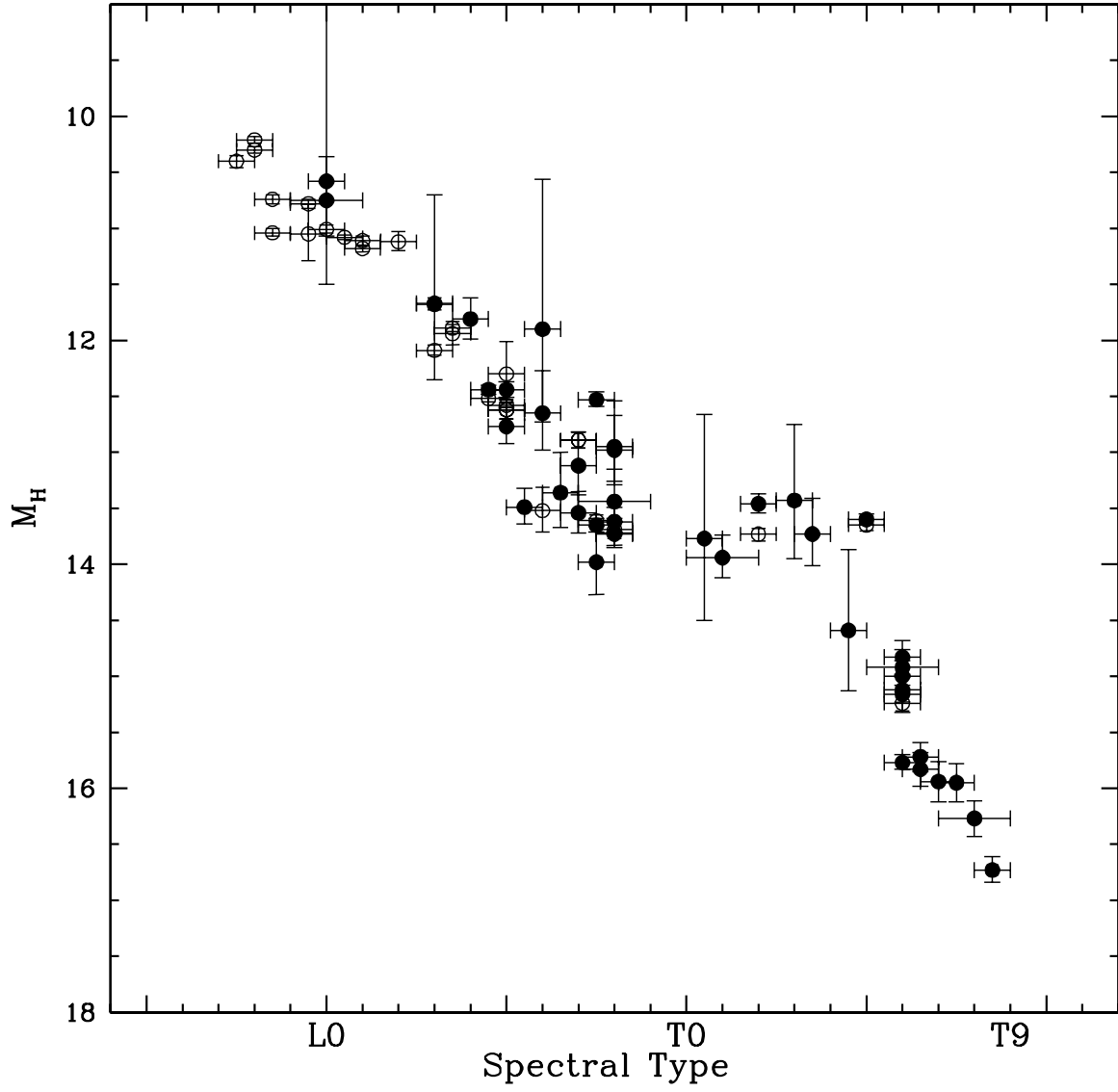


Fig. 3.— Same as for Figure 2, except that absolute H-band magnitude (M_H) is plotted versus spectral type.

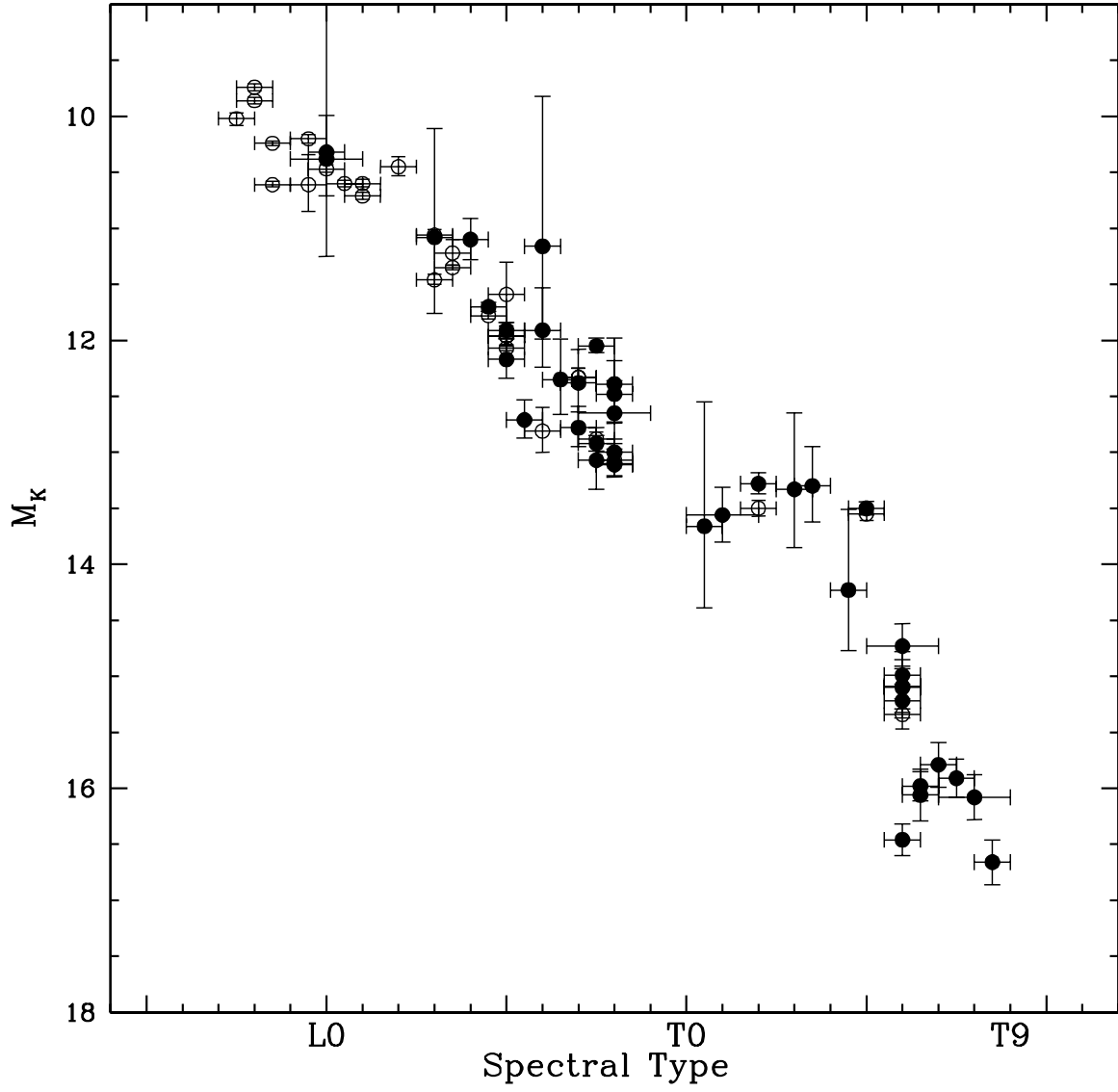


Fig. 4.— Same as for Figure 2, except that absolute K-band magnitude (M_K) is plotted versus spectral type.

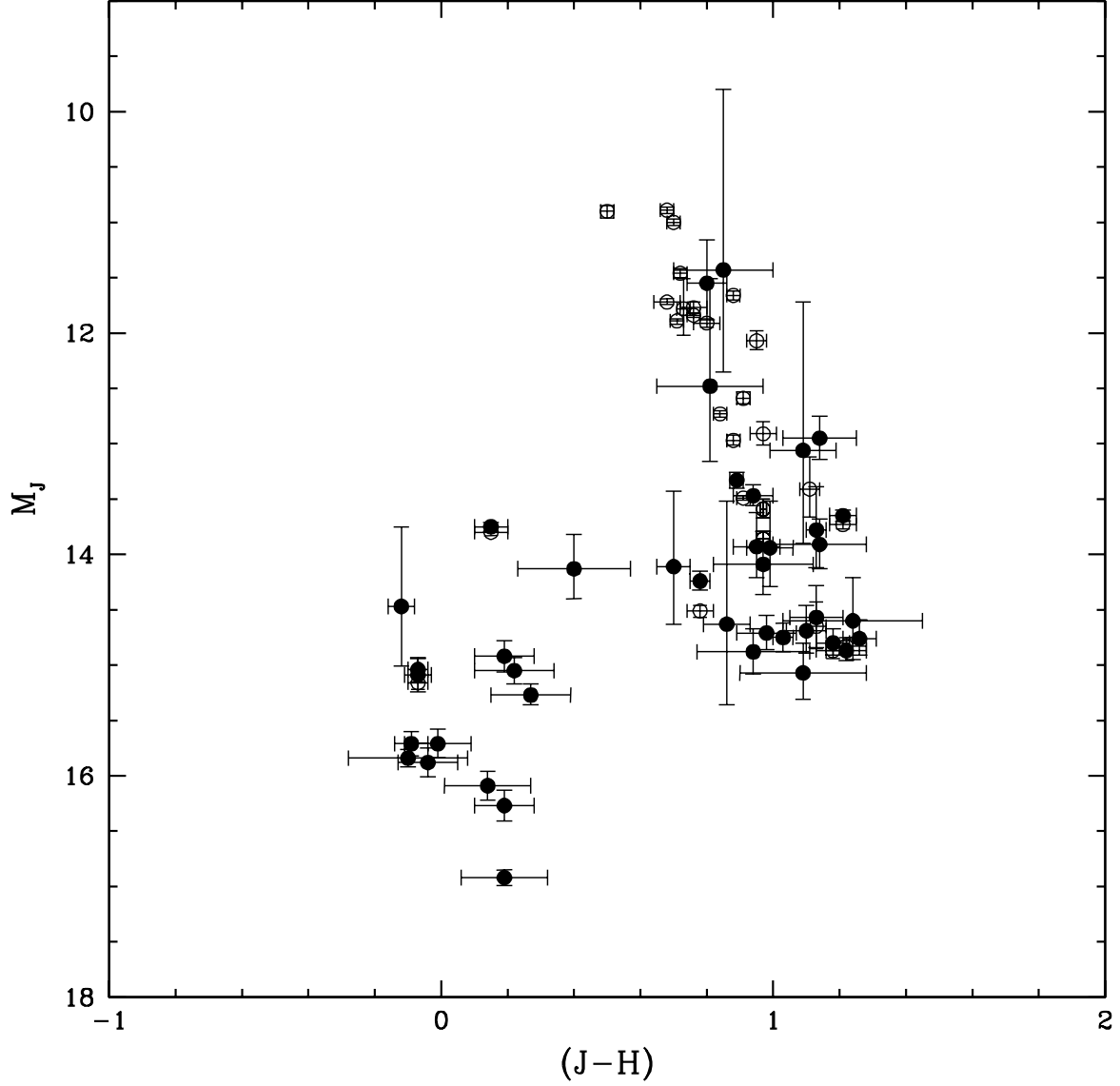


Fig. 5.— Absolute J-band magnitude (M_J) is plotted versus $(J - H)$ color. The solid data points are the results from the infrared astrometry and photometry from Tables 2 and 6 of this paper, while the open points are the results of optical astrometry and infrared photometry from D02. For the seven objects in common, results are plotted for both optical and infrared parallaxes. A complete description of this figure is given in §14.2.

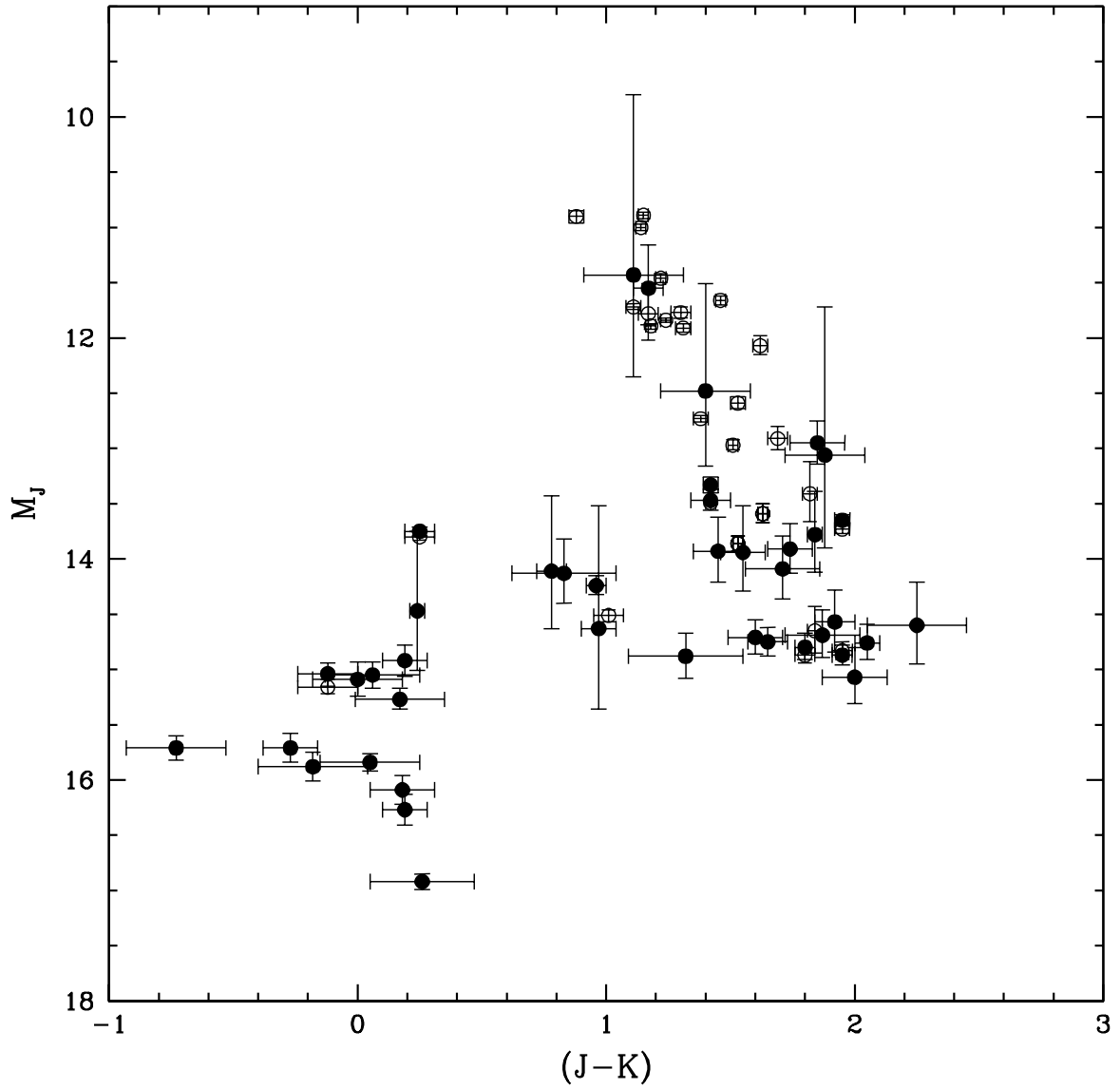


Fig. 6.— Same as for Figure 5, except that M_J is plotted versus $(J - K)$ color.

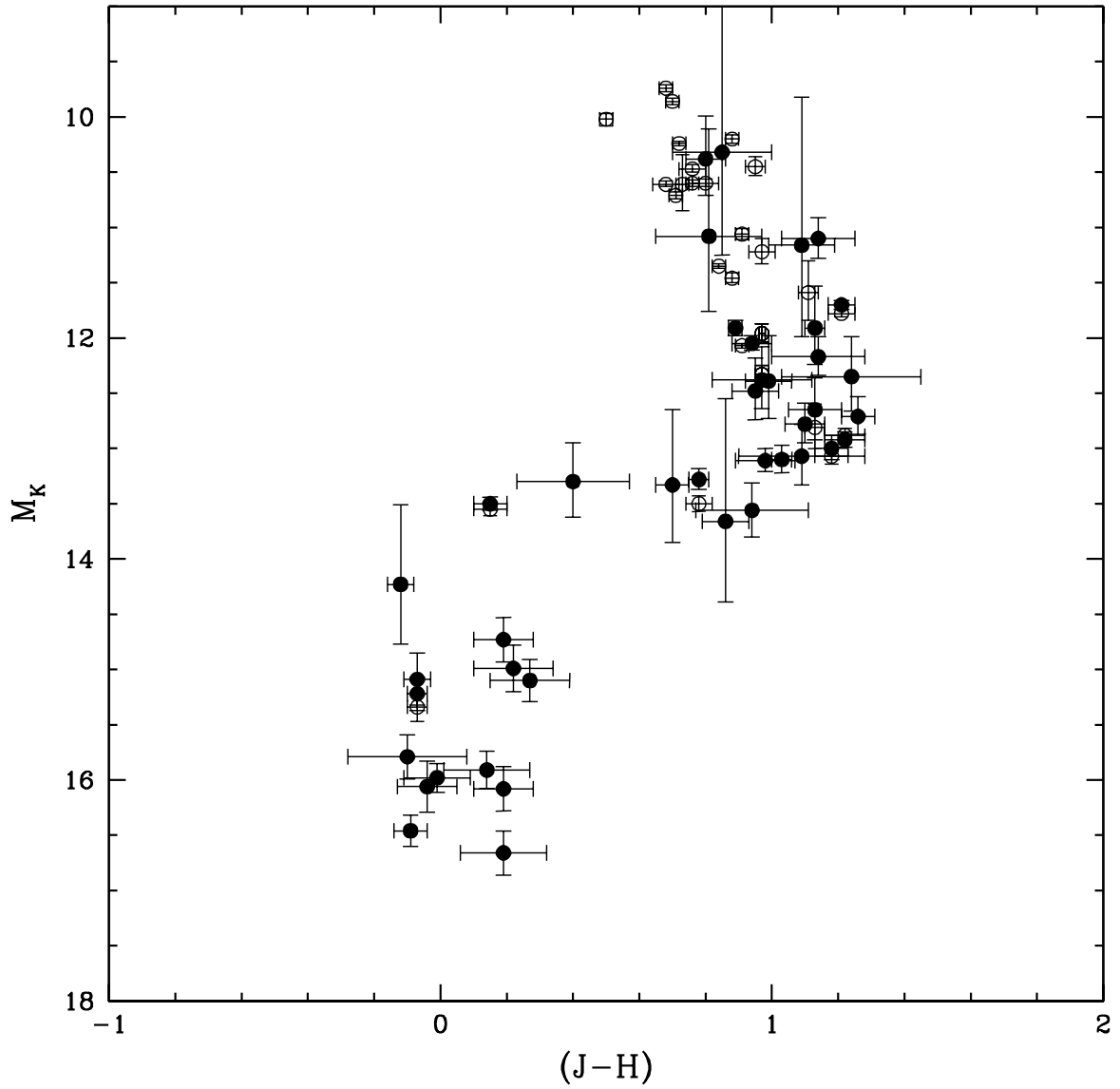


Fig. 7.— Same as for Figure 5, except that M_K is plotted versus $(J - H)$ color.

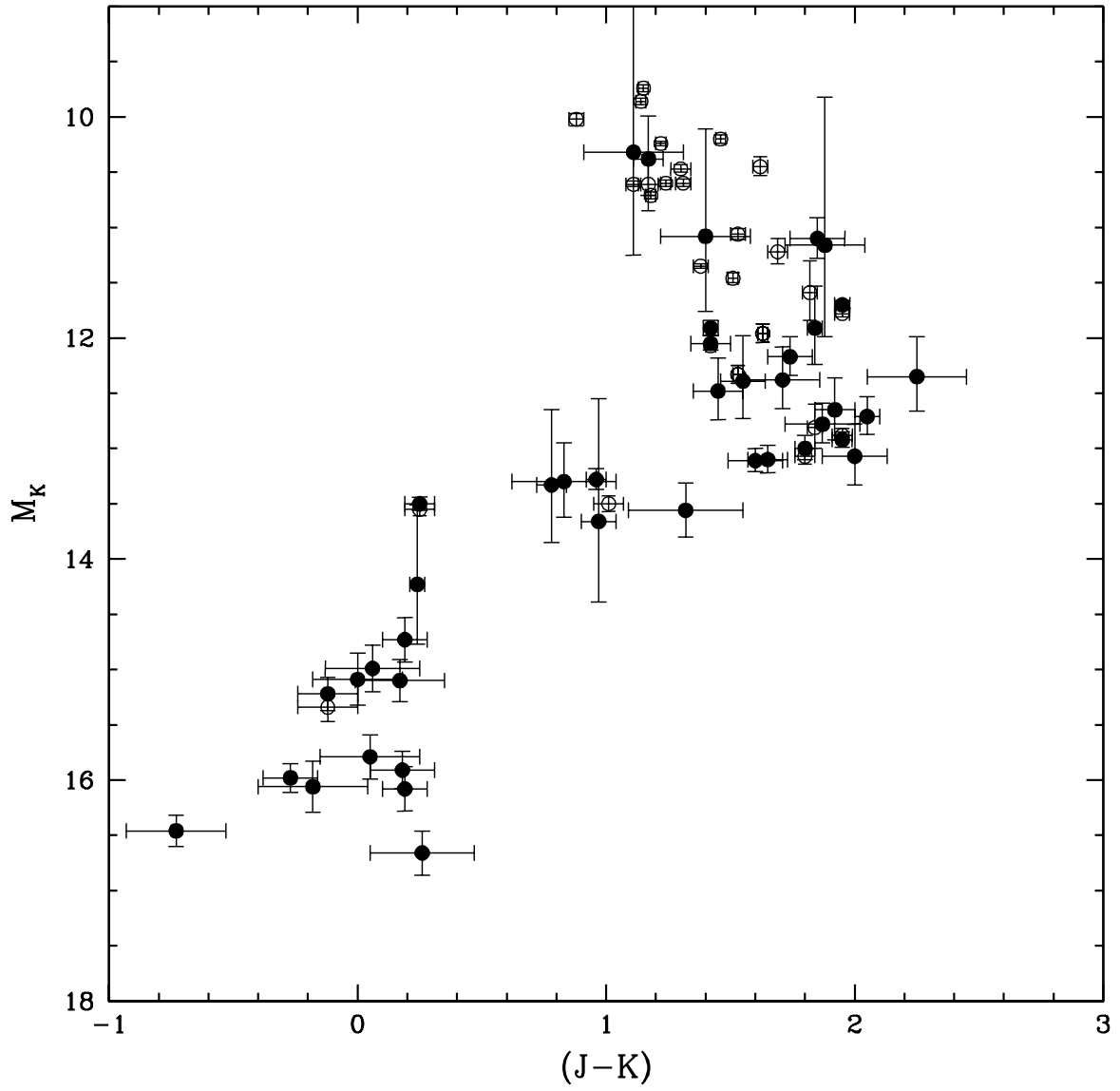


Fig. 8.— Same as for Figure 5, except that M_K is plotted versus $(J - K)$ color.

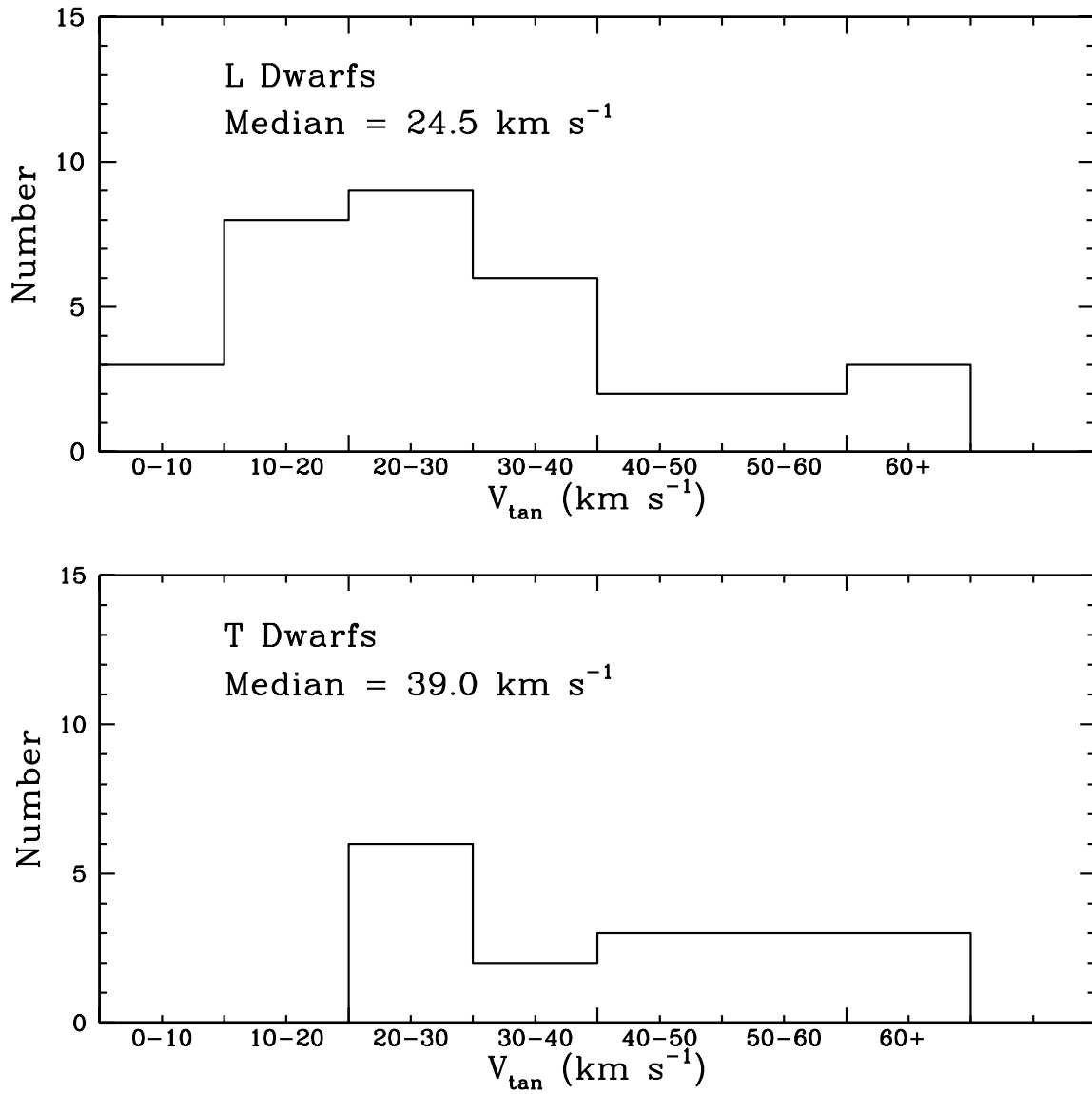


Fig. 9.— Histograms of the distributions of V_{tan} for L dwarfs and T dwarfs.

Table 1. Observations and Reference Stars.

Star	Sp.T.	Filt.	No. Nights	Δt (yrs)	Mean Epoch	No. Ref. Stars	Rel.→Abs.
2MASS J00303013–1450333	L7	H	31	2.18	2001.800	10	IR
SDSS J003259.37+141037.1	L8	H	23	2.02	2002.159	14	H,S,IR
SDSS J010752.42+004156.3	L5.5	H	34	1.87	2002.308	6	H,S
SDSS J015141.69+124429.6	T1±1	H	26	2.03	2002.216	12	H,S,IR
SDSS J020742.83+000056.2	T4.5	H	20	1.93	2002.218	9	H,S,IR
2MASS J02431371–2453298	T6	J	26	2.20	2001.774	5	IR
2MASS J03284265+2302051	L8	H	22	2.19	2001.745	9	IR
2MASS J04151954–0935066	T8/T9	J	20	2.12	2002.035	5	IR
SDSS J042348.57–041403.5	L7.5/T0	H	21	2.02	2002.248	9	IR
SDSS J053952.00–005901.9	L5	H	22	2.02	2001.970	10	IR
2MASS J05591914–1404488	T5	J	27	2.10	2001.875	14	IR
2MASS J07271824+1710012	T7	J	28	2.02	2001.906	17	IR
2MASS J08251968+2115521	L7.5	H	16	1.88	2001.926	14	IR
SDSS J083008.12+482847.4	L8	H	11	1.87	2001.969	11	H,S
SDSS J083717.21–000018.0	T0.5	J	10	1.78	2002.016	12	H,S,IR
2MASS J08503593+1057156AB	L6+L/T	H	13	1.86	2001.791	8	IR
2MASS J09373487+2931409	T6p	J	14	1.87	2001.984	6	IR
2MASS J09510549+3558021	L6	H	15	1.28	2001.725	9	IR
SDSS J102109.69–030420.1	T3	J	15	1.31	2001.743	8	H,S,IR
2MASS J10475385+2124234	T6.5	J	22	1.32	2001.739	7	IR
2MASS J12171110–0311131	T7.5	J	18	1.30	2001.848	4	H,S,IR
2MASS J12255432–2739466AB	T6:+T8:	J	14	1.30	2001.919	12	IR
2MASS J12373919+6526148	T6.5e	J	13	1.38	2001.802	6	H,S,IR
SDSS J125453.90–012247.4	T2	J	15	1.29	2001.905	13	H,S,IR
SDSS 132629.81–003831.4	L8?	H	17	1.38	2001.829	10	H,S,IR
SDSS J134646.43–003150.4	T6	J	22	1.39	2001.901	9	H,S,IR
SDSS J143517.20–004612.9	L0	H	24	1.39	2001.925	4	H,S
SDSS J143535.72–004347.0	L3	H	24	1.39	2001.923	6	H,S
SDSS J144600.60+002452.0	L5	H	25	1.36	2001.916	5	H,S
2MASS J15232263+3014562	L8	H	32	1.36	2001.888	10	IR
SDSS J162414.36+002915.8	T6	J	24	1.37	2001.920	6	H,S
2MASS J16322911+1904407	L8	H	22	1.38	2001.852	8	IR
2MASS J17114573+2232044	L6.5	H	26	1.36	2001.983	16	H,S,IR
2MASS J17281150+3948593AB	L7+L/T	H	24	1.38	2001.978	11	IR
SDSS J175032.96+175903.9	T3.5	J	29	1.24	2001.077	26	H,S,IR
2MASS J18410861+3117279	L4pec	H	39	2.03	2002.048	19	IR
2MASS J21011544+1756586AB	L7.5+L8?	H	48	2.18	2002.055	17	IR
2MASS J22244381–0158521	L4.5	H	50	2.20	2001.969	6	IR
SDSS J225529.09–003433.4	L0:	H	44	2.10	2002.101	13	H,S

Table 1—Continued

Star	Sp.T.	Filt.	No. Nights	Δt (yrs)	Mean Epoch	No. Ref. Stars	Rel.→Abs.
2MASS J23565477-1553111	T6	J	43	2.20	2001.939	10	IR

Table 2. Astrometric Results.

Star	Sp.T.	π_{rel} (mas)	π_{abs} (mas)	μ_{rel} (mas yr ⁻¹)	P.A. (deg)	V_{tan} (km s ⁻¹)
2MASS J003030–1450	L7	35.39 ± 4.49	37.42 ± 4.50	246.6 ± 3.6	96.56 ± 0.42	31.2 ± 3.8
SDSS J003259+1410	L8	28.82 ± 5.16	30.14 ± 5.16	275.8 ± 6.9	81.83 ± 0.72	43.4 ± 7.7
SDSS J010752+0041	L5.5	61.98 ± 4.48	64.13 ± 4.51	634.5 ± 7.1	81.71 ± 0.32	46.9 ± 3.3
SDSS J015141+1244	T1±1	45.26 ± 3.36	46.73 ± 3.37	742.7 ± 4.2	92.84 ± 0.16	75.3 ± 5.5
SDSS J020742+0000	T4.5	33.15 ± 9.86	34.85 ± 9.87	156.3 ± 11.4	96.29 ± 2.09	21.3 ± 6.7
2MASS J024313–2453	T6	90.23 ± 3.50	93.62 ± 3.63	354.8 ± 4.1	234.20 ± 0.33	18.0 ± 0.7
2MASS J032842+2302	L8	31.06 ± 4.19	33.13 ± 4.20	61.0 ± 4.9	168.08 ± 2.30	8.7 ± 1.3
2MASS J041519–0935	T8/T9	172.87 ± 2.75	174.34 ± 2.76	2255.3 ± 3.2	76.48 ± 0.04	61.4 ± 1.0
SDSS J042348–0414	L7.5/T0	64.50 ± 1.69	65.93 ± 1.70	333.1 ± 2.8	284.23 ± 0.24	24.0 ± 0.6
SDSS J053952–0059	L5	74.43 ± 2.16	76.12 ± 2.17	356.1 ± 3.5	27.49 ± 0.28	22.2 ± 0.7
2MASS J055919–1404	T5	93.84 ± 1.43	95.53 ± 1.44	655.2 ± 2.8	121.10 ± 0.12	32.5 ± 0.5
2MASS J072718+1710	T7	109.01 ± 2.34	110.14 ± 2.34	1296.5 ± 4.5	126.25 ± 0.10	55.8 ± 1.2
2MASS J082519+2115	L7.5	94.20 ± 1.83	95.64 ± 1.84	584.5 ± 4.0	239.45 ± 0.20	29.0 ± 0.6
SDSS J083008+4828	L8	74.93 ± 3.42	76.42 ± 3.43	1267.0 ± 6.5	232.58 ± 0.15	78.6 ± 3.6
SDSS J083717–0000	T0.5	32.44 ± 13.45	33.70 ± 13.45	173.0 ± 16.7	185.05 ± 2.76	24.3 ± 11.8
2MASS J085035+1057AB	L6+L/T	24.76 ± 4.21	26.22 ± 4.21	147.2 ± 6.2	261.93 ± 1.20	26.6 ± 4.5
2MASS J093734+2931	T6p	161.47 ± 3.87	162.84 ± 3.88	1622.0 ± 7.1	143.14 ± 0.13	47.2 ± 1.1
2MASS J095105+3558	L6	14.88 ± 7.40	16.09 ± 7.40	189.4 ± 10.6	211.83 ± 1.60	55.8 ± 32.7
SDSS J102109–0304	T3	39.13 ± 11.00	40.78 ± 11.00	179.4 ± 15.2	246.24 ± 2.42	20.9 ± 6.3
2MASS J104753+2124	T6.5	92.82 ± 3.76	94.73 ± 3.81	1728.4 ± 7.7	254.08 ± 0.13	86.5 ± 3.5
2MASS J121711–0311	T7.5	108.63 ± 5.87	110.36 ± 5.88	1061.8 ± 10.2	274.95 ± 0.27	45.6 ± 2.5
2MASS J122554–2739AB	T6:+T8:	72.76 ± 3.46	74.20 ± 3.47	736.9 ± 6.8	147.80 ± 0.26	47.1 ± 2.3
2MASS J123739+6526	T6.5e	93.82 ± 4.75	96.07 ± 4.78	1131.4 ± 8.9	242.33 ± 0.23	55.8 ± 2.8
SDSS J125453–0122	T2	74.51 ± 2.87	75.71 ± 2.88	483.2 ± 6.1	284.45 ± 0.36	30.3 ± 1.2
SDSS J132629–0038	L8?	49.01 ± 6.33	49.98 ± 6.33	250.6 ± 8.9	244.63 ± 1.02	23.8 ± 3.2
SDSS J134646–0031	T6	71.13 ± 5.01	72.74 ± 5.02	491.5 ± 10.0	254.31 ± 0.58	32.0 ± 2.3
SDSS J143517–0046	L0	8.42 ± 5.10	9.85 ± 5.18	24.7 ± 9.2	64.99 ± 10.65	11.9 ± 9.7
SDSS J143535–0043	L3	15.28 ± 5.76	16.07 ± 5.76	107.5 ± 8.8	168.27 ± 2.34	31.7 ± 13.3
SDSS J144600+0024	L5	43.04 ± 3.21	45.46 ± 3.25	191.2 ± 7.0	110.06 ± 1.05	19.9 ± 1.6
2MASS J152322+3014	L8	55.77 ± 3.27	57.30 ± 3.27	221.4 ± 5.9	139.77 ± 0.76	18.3 ± 1.2
SDSS J162414+0029	T6	84.94 ± 3.82	86.85 ± 3.85	374.0 ± 6.0	269.65 ± 0.46	20.4 ± 1.0
2MASS J163229+1904	L8	62.17 ± 3.31	63.58 ± 3.32	301.7 ± 5.1	101.37 ± 0.48	22.5 ± 1.2
2MASS J171145+2232	L6.5	31.48 ± 4.80	33.11 ± 4.81	31.2 ± 7.5	98.35 ± 6.88	4.5 ± 1.2
2MASS J172811+3948AB	L7+L/T	40.33 ± 3.26	41.49 ± 3.26	45.0 ± 6.4	125.17 ± 4.07	5.1 ± 0.9
SDSS J175033+1759	T3.5	35.07 ± 4.53	36.24 ± 4.53	204.3 ± 7.8	60.80 ± 1.09	26.7 ± 3.5
2MASS J184108+3117	L4pec	22.12 ± 1.88	23.57 ± 1.89	72.6 ± 3.7	55.00 ± 1.46	14.6 ± 1.4
2MASS J210115+1756AB	L7.5+L8?	29.04 ± 3.42	30.14 ± 3.42	208.5 ± 3.7	136.33 ± 0.51	32.8 ± 3.8
2MASS J222443–0158	L4.5	83.43 ± 1.46	85.01 ± 1.50	980.6 ± 2.0	151.35 ± 0.06	54.7 ± 1.0

Table 2—Continued

Star	Sp.T.	π_{rel} (mas)	π_{abs} (mas)	μ_{rel} (mas yr ⁻¹)	P.A. (deg)	V_{tan} (km s ⁻¹)
SDSS J225529–0034	L0:	14.61 ± 2.56	16.19 ± 2.59	179.9 ± 2.6	191.61 ± 0.41	52.7 ± 8.7
2MASS J235654–1553	T6	66.96 ± 3.38	68.97 ± 3.42	746.2 ± 2.9	216.46 ± 0.11	51.3 ± 2.6

Table 3. Comparison of USNO Infrared and Optical Results.

Star	Program	Δt (yrs)	π_{abs} (mas)	μ_{rel} (mas yr ⁻¹)	P.A. (deg)
2MASS J055919–1404	CCD ¹	2.1	97.7 ± 1.3	661.2 ± 1.2	121.6 ± 0.1
	IR	2.10	95.53 ± 1.44	655.2 ± 2.8	121.10 ± 0.12
	CCD-IR		$+2.2 \pm 1.9$	$+6.0 \pm 3.0$	-0.5 ± 0.2
2MASS J082519+2115	CCD ¹	2.0	93.8 ± 1.0	585.6 ± 1.4	240.5 ± 0.2
	IR	1.88	95.64 ± 1.84	584.5 ± 4.0	239.45 ± 0.20
	CCD-IR		-1.8 ± 2.1	$+1.1 \pm 4.2$	$+1.0 \pm 0.3$
2MASS J085035+1057AB	CCD ¹	3.3	39.1 ± 3.5	144.7 ± 2.0	267.0 ± 0.9
	IR	1.86	26.22 ± 4.21	147.2 ± 6.2	261.93 ± 1.20
	CCD-IR		$+12.9 \pm 5.5$	-2.5 ± 6.5	$+5.1 \pm 1.5$
SDSS J125453–0122	CCD ¹	1.2	84.9 ± 1.9	496.1 ± 1.8	285.2 ± 0.4
	IR	1.29	75.71 ± 2.88	483.2 ± 6.1	284.45 ± 0.36
	CCD-IR		$+9.2 \pm 3.4$	$+12.9 \pm 6.4$	$+0.7 \pm 0.6$
SDSS J162414+0029	CCD ¹	2.2	91.5 ± 2.3	383.2 ± 1.9	269.6 ± 0.5
	IR	1.37	86.85 ± 3.85	374.0 ± 6.0	269.65 ± 0.46
	CCD-IR		$+4.6 \pm 4.5$	$+9.2 \pm 6.3$	-0.0 ± 0.7
2MASS J163229+1904	CCD ¹	3.2	65.6 ± 2.1	298.0 ± 0.9	100.4 ± 0.2
	IR	1.38	63.58 ± 3.32	301.7 ± 5.1	101.37 ± 0.48
	CCD-IR		$+2.0 \pm 3.9$	-3.7 ± 5.2	-1.0 ± 0.5
2MASS J222443–0158	CCD ¹	2.3	88.1 ± 1.1	983.8 ± 0.7	152.3 ± 0.1
	IR	2.20	85.01 ± 1.50	980.6 ± 2.0	151.35 ± 0.06
	CCD-IR		$+3.1 \pm 1.9$	$+3.8 \pm 2.1$	$+0.9 \pm 0.2$
Weighted Mean Diff.			$+2.6 \pm 1.4$	$+3.9 \pm 1.5$	$+0.3 \pm 0.1$

¹D02

Table 4. Comparison of Infrared Astrometric Results.

Star	Program	Δt (yrs)	π_{rel} (mas)	μ_{rel} (mas yr ⁻¹)	P.A. (deg)
SDSS J102109–0304	USNO	1.31	39.13 ± 11.00	179.4 ± 15.2	246.24 ± 2.42
	ESO ¹	1.7	34.4 ± 4.6	183.2 ± 3.4	248.8 ± 1.0
	U–E		+4.7 ± 11.9	–3.8 ± 15.6	–2.6 ± 2.6
2MASS J104753+2124	USNO	1.32	92.82 ± 3.76	1728.4 ± 7.7	254.08 ± 0.13
	ESO ¹	1.9	110.8 ± 6.6	1698.9 ± 2.5	256.4 ± 0.1
	U–E		–18.0 ± 7.6	+29.5 ± 8.1	–2.3 ± 0.2
2MASS J121711–0311	USNO	1.30	108.63 ± 5.87	1061.8 ± 10.2	274.95 ± 0.27
	ESO ¹	1.9	90.8 ± 2.2	1057.1 ± 1.7	274.1 ± 0.1
	U–E		+17.8 ± 6.3	+4.7 ± 10.3	+0.9 ± 0.3
2MASS J122554–2739AB	USNO	1.30	72.76 ± 3.46	736.9 ± 6.8	147.80 ± 0.26
	ESO ¹	1.9	75.1 ± 2.5	736.8 ± 2.9	148.5 ± 0.1
	U–E		–2.3 ± 4.3	+0.1 ± 7.4	–0.7 ± 0.3
SDSS J125453–0122	USNO	1.29	74.51 ± 2.87	483.2 ± 6.1	284.45 ± 0.36
	ESO ¹	1.7	73.2 ± 1.9	491.0 ± 2.5	284.7 ± 0.1
	U–E		+1.3 ± 3.4	–7.8 ± 6.6	–0.3 ± 0.4
SDSS J134646–0031	USNO	1.39	71.13 ± 5.01	491.5 ± 10.0	254.31 ± 0.58
	ESO ¹	1.7	68.3 ± 2.3	516.0 ± 3.3	257.2 ± 0.2
	U–E		+2.8 ± 5.5	–24.5 ± 10.5	–2.9 ± 0.6
SDSS J162414+0029	USNO	1.37	84.94 ± 3.82	374.0 ± 6.0	269.65 ± 0.46
	ESO ¹	1.9	90.9 ± 1.2	373.0 ± 1.6	268.6 ± 0.3
	U–E		–6.0 ± 4.0	+1.0 ± 6.2	1.1 ± 0.5
Weighted Mean Diff. (USNO-ESO)			–0.4 ± 3.1	+1.0 ± 5.7	–1.0 ± 0.6

¹TBK03

Table 5. Additional USNO *JHK* Photometry.

Star	Sp.T.	$K \pm \sigma(K)$	$J - H \pm \sigma(J - H)$	$H - K \pm \sigma(H - K)$
SDSS J020742+0000*	T4.5	16.52 ± 0.03	-0.12 ± 0.04	0.24 ± 0.03
SDSS J053952-0059	L5	12.49 ± 0.04	0.89 ± 0.04	0.55 ± 0.05
2MASS J093734+2931	T6p	15.55 ± 0.15	-0.12 ± 0.05	-0.85 ± 0.15
2MASS J095105+3558	L6	15.10 ± 0.12	1.04 ± 0.13	0.77 ± 0.16
2MASS J104753+2124	T6.5	16.10 ± 0.10	-0.12 ± 0.16	-0.20 ± 0.16
SDSS J134646-0031	T6	15.76 ± 0.23	-0.07 ± 0.04	0.12 ± 0.16
SDSS J162414+0029	T6	15.53 ± 0.12	-0.08 ± 0.03	-0.04 ± 0.12
2MASS J172811+3948AB	L7+L/T	13.96 ± 0.11	1.06 ± 0.07	0.60 ± 0.10
2MASS J210115+1756AB	L7.5+L8?	16.90 ± 0.10

*Based on relative photometry of 2MASS stars in the ASTROCAM field of view

Table 6. Adopted Spectral Types and JHK Photometry.

Star	Sp.T.	Spec. Ref.	$K \pm \sigma(K)$	$(J - H) \pm \sigma(J - H)$	$(J - K) \pm \sigma(J - K)$	Phot. Ref.
2MASS J 003030–1450	L7	1	14.51 ± 0.10	0.97 ± 0.15	1.71 ± 0.15	A
SDSS J003259+1410	L8	3	14.99 ± 0.05	0.99 ± 0.07	1.55 ± 0.09	A,B
SDSS J010752+0041	L5.5	3	13.67 ± 0.07	1.26 ± 0.05	2.05 ± 0.05	A,B
SDSS J015141+1244	T1±1	3	15.21 ± 0.19	0.94 ± 0.17	1.32 ± 0.23	A
SDSS J020742+0000	T4.5	3	16.52 ± 0.03	-0.12 ± 0.04	0.24 ± 0.03	D
2MASS J024313–2453	T6	2	15.24 ± 0.17	0.27 ± 0.12	0.17 ± 0.18	A
2MASS J032842+2302	L8	1	14.88 ± 0.05	0.95 ± 0.07	1.45 ± 0.10	A,B
2MASS J041519–0935	T8/T9	2,4	15.45 ± 0.20	0.19 ± 0.13	0.26 ± 0.21	A
SDSS J042348–0414	L7.5/T0	3,5,6	12.95 ± 0.03	0.94 ± 0.06	1.42 ± 0.08	A,B
SDSS J053952–0059	L5	11	12.50 ± 0.04	0.89 ± 0.02	1.42 ± 0.03	A,D,E
2MASS J055919–1404	T5	14	13.60 ± 0.05	0.15 ± 0.05	0.25 ± 0.06	A
2MASS J072718+1710	T7	2	15.58 ± 0.19	-0.10 ± 0.18	0.05 ± 0.20	A
2MASS J082519+2115	L7.5	1	13.02 ± 0.05	1.22 ± 0.06	1.95 ± 0.04	A,B,C
SDSS J083008+4828	L8	3,5	13.69 ± 0.03	0.98 ± 0.09	1.60 ± 0.11	A,B
SDSS J083717–0000	T0.5	3,16	16.02 ± 0.05	0.86 ± 0.07	0.97 ± 0.07	E
2MASS J085035+1057AB	L6+L/T	13,15	14.45 ± 0.04	1.13 ± 0.03	1.84 ± 0.03	A,B,C
2MASS J093734+2931	T6p	2	15.40 ± 0.13	-0.09 ± 0.05	-0.73 ± 0.20	A,D
2MASS J095105+3558	L6	1	15.13 ± 0.10	1.09 ± 0.10	1.88 ± 0.16	A,D
SDSS J102109–0304	T3	3,16	15.28 ± 0.05	0.70 ± 0.05	0.78 ± 0.06	A,E
2MASS J104753+2124	T6.5	7	16.10 ± 0.10	-0.01 ± 0.10	-0.27 ± 0.11	A,D
2MASS J121711–0311	T7.5	7	15.70 ± 0.12	0.14 ± 0.13	0.18 ± 0.13	A,C
2MASS J122554–2739A	T6:	7,10,12	15.38 ± 0.17	0.19 ± 0.09	0.19 ± 0.16	A,F
2MASS J122554–2739B	T8:	7,10,12	16.73 ± 0.17	0.19 ± 0.09	0.19 ± 0.16	A,F
2MASS J123739+6526	T6.5e	7	16.15 ± 0.20	-0.04 ± 0.09	-0.18 ± 0.22	A,C
SDSS J125453–0122	T2	3,16	13.88 ± 0.04	0.78 ± 0.03	0.96 ± 0.04	A,E
SDSS J132629–0038	L8?	11	14.16 ± 0.05	1.13 ± 0.08	1.92 ± 0.08	A,B
SDSS J134646–0031	T6	3,19	15.78 ± 0.18	-0.07 ± 0.04	0.00 ± 0.18	A,D
SDSS J143517–0046	L0	8	15.35 ± 0.18	0.85 ± 0.15	1.11 ± 0.20	A
SDSS J143535–0043	L3	8	15.05 ± 0.14	0.81 ± 0.16	1.40 ± 0.18	A
SDSS J144600+0024	L5	2,3	13.88 ± 0.08	1.14 ± 0.14	1.74 ± 0.09	A,B
2MASS J152322+3014	L8	1	14.31 ± 0.03	1.03 ± 0.03	1.65 ± 0.08	A,B,C
SDSS J162414+0029	T6	3,20	15.53 ± 0.12	-0.07 ± 0.03	-0.12 ± 0.12	A,D
2MASS J163229+1904	L8	13	13.98 ± 0.03	1.18 ± 0.05	1.80 ± 0.04	A,B,C
2MASS J171145+2232	L6.5	1	14.75 ± 0.10	1.24 ± 0.21	2.25 ± 0.20	A
2MASS J172811+3948AB	L7+L/T	1,17	13.94 ± 0.05	1.10 ± 0.06	1.87 ± 0.15	A,D
SDSS J175033+1759	T3.5	3	15.50 ± 0.19	0.40 ± 0.17	0.83 ± 0.21	A
2MASS J184108+3117	L4pec	1	14.24 ± 0.07	1.14 ± 0.11	1.85 ± 0.11	A
2MASS J210115+1756AB	L7.5+L8?	1,18	14.92 ± 0.12	1.09 ± 0.19	2.00 ± 0.13	A,D

Table 6—Continued

Star	Sp.T.	Spec. Ref.	$K \pm \sigma(K)$	$(J - H) \pm \sigma(J - H)$	$(J - K) \pm \sigma(J - K)$	Phot. Ref.
2MASS J222443–0158	L4.5	1	12.05 ± 0.02	1.21 ± 0.04	1.95 ± 0.03	A
SDSS J225529–0034	L0:	9	14.33 ± 0.08	0.80 ± 0.06	1.17 ± 0.06	A,B
2MASS J235654–1553	T6	2	15.80 ± 0.18	0.22 ± 0.12	0.06 ± 0.19	A

References. — (1) Kirkpatrick et al. (2000); (2) Burgasser et al. (2002a); (3) Geballe et al. (2002); (4) Knapp et al. (2004); (5) Kirkpatrick (2004); (6) See §15.2; (7) Burgasser et al. (1999); (8) Hawley et al. (2002); (9) Schneider et al. (2002); (10) Burgasser et al. (2003); (11) Fan et al. (2000); (12) See §15.6; (13) Kirkpatrick et al. (1999); (14) Burgasser et al. (2000); (15) See §15.4; (16) Leggett et al. (2000); (17) See §15.8; (18) See §15.9; (19) Tsvetanov et al. (2000); (20) Strauss et al. (1999); (A) 2MASS All-Sky Point Source Catalog; (B) Leggett et. al (2002); (C) D02; (D) Table 5, this paper; (E) Leggett et. al (2000); (F) See §15.6

Table 7. Infrared Absolute Magnitudes based on USNO Astrometry.

Star	Sp.T.	Opt/IR	M_J	$\sigma(-)$	$\sigma(+)$	M_H	$\sigma(-)$	$\sigma(+)$	M_K	$\sigma(-)$	$\sigma(+)$
2MASS J034543+2540	L0	O	11.77	.05	.05	11.01	.04	.03	10.47	.04	.03
SDSS J143517-0046	L0	I	11.43	1.63	.92	10.58	1.63	.92	10.32	1.63	.93
SDSS J225529-0034	L0:	I	11.55	.39	.33	10.75	.39	.32	10.38	.39	.33
2MASS J074642+2000A	L0.5	O	11.84	.02	.02	11.08	.02	.02	10.60	.03	.03
2MASS J143928+1929	L1	O	11.89	.02	.03	11.18	.02	.03	10.71	.03	.03
2MASS J165803+7027	L1	O	11.91	.04	.04	11.11	.04	.04	10.60	.04	.03
Kelu-1	L2	O	12.07	.09	.08	11.12	.09	.08	10.45	.09	.08
DENIS J1058.7-1548	L3	O	12.97	.05	.04	12.09	.05	.04	11.46	.05	.04
2MASS J114634+2230A	L3	O	12.59	.06	.05	11.68	.06	.05	11.06	.05	.05
2MASS J143535-0043	L3	I	12.48	.97	.68	11.67	.97	.68	11.08	.97	.68
2MASS J003616+1821	L3.5	O	12.73	.03	.03	11.89	.03	.03	11.35	.02	.02
2MASS J032613+2950	L3.5	O	12.91	.11	.10	11.94	.11	.10	11.22	.12	.11
2MASS J184108+3117	L4pec	I	12.95	.20	.19	11.81	.19	.18	11.10	.19	.18
2MASS J222443-0158	L4.5	I+O	13.70	.05	.05	12.49	.04	.04	11.75	.04	.04
SDSS J053952-0059	L5	I	13.33	.07	.07	12.44	.07	.07	11.91	.07	.07
DENIS J122815-1547A	L5	O	13.59	.09	.08	12.62	.09	.08	11.96	.09	.08
DENIS J122815-1547B	L5	O	13.59	.09	.08	12.62	.09	.08	11.96	.09	.08
2MASS J132855+2114	L5	O	13.41	.29	.25	12.30	.29	.25	11.59	.29	.25
SDSS J144600+0024	L5	I	13.91	.23	.22	12.77	.17	.15	12.17	.18	.17
2MASS J150747-1627	L5	O	13.49	.02	.02	12.58	.02	.02	12.07	.02	.02
SDSS J010752+0041	L5.5	I	14.76	.17	.15	13.49	.17	.15	12.71	.18	.16
2MASS J085035+1057A	L6	I+O	14.34	.46	.38	13.21	.45	.37	12.50	.45	.37
2MASS J095105+3558	L6	I	13.06	1.34	.84	11.90	1.34	.83	11.16	1.34	.83
2MASS J171145+2232	L6.5	I	14.60	.39	.35	13.36	.36	.31	12.35	.36	.31
2MASS J003030-1450	L7	I	14.09	.30	.27	13.12	.30	.26	12.38	.30	.26
2MASS J172811+3948A	L7	I	14.69	.23	.20	13.54	.19	.18	12.78	.19	.17
DENIS J020529-1159A	L7	O	13.86	.07	.07	12.89	.07	.07	12.33	.08	.08
DENIS J020529-1159B	L7	O	13.86	.07	.07	12.89	.07	.07	12.33	.08	.08
SDSS J042348-0414	L7.5/T0	I	13.47	.10	.09	12.53	.07	.06	12.05	.07	.06
2MASS J082519+2115	L7.5	I+O	14.84	.08	.08	13.62	.04	.04	12.89	.05	.05
2MASS J210115+1756A	L7.5	I	15.07	.27	.24	13.98	.32	.29	13.07	.29	.26
SDSS J003259+1410	L8	I	13.94	.42	.35	12.95	.41	.34	12.39	.41	.34
2MASS J032842+2302	L8	I	13.93	.31	.28	12.98	.31	.28	12.48	.30	.26
SDSS J083008+4828	L8	I	14.71	.16	.15	13.73	.11	.10	13.11	.11	.10
SDSS J132629-0038	L8?	I	14.57	.29	.27	13.44	.29	.27	12.65	.29	.27
2MASS J152322+3014	L8	I	14.75	.13	.13	13.72	.13	.13	13.10	.13	.12
2MASS J163229+1904	L8	I+O	14.85	.08	.07	13.67	.08	.07	13.05	.07	.06
SDSS J083717-0000	T0.5	I	14.63	1.11	.73	13.77	1.11	.73	13.66	1.11	.73
SDSS J015141+1244	T1±1	I	14.88	.21	.20	13.94	.20	.18	13.56	.25	.24
SDSS J125453-0122	T2	I+O	14.41	.12	.12	13.63	.12	.12	13.45	.12	.12
SDSS J102109-0304	T3	I	14.11	.68	.52	13.43	.68	.52	13.33	.68	.52
SDSS J175033+1759	T3.5	I	14.13	.31	.27	13.73	.32	.28	13.30	.35	.32
SDSS J020742+0000	T4.5	I	14.47	.72	.54	14.59	.72	.54	14.23	.72	.54
2MASS J055919-1404	T5	I+O	13.78	.03	.03	13.63	.04	.04	13.53	.05	.06
2MASS J024313-2453	T6	I	15.27	.10	.09	15.00	.14	.14	15.10	.19	.19
2MASS J093734+2931	T6p	I	15.71	.11	.11	15.77	.07	.06	16.46	.14	.14

Table 7—Continued

Star	Sp.T.	Opt/IR	M_J	$\sigma(-)$	$\sigma(+)$	M_H	$\sigma(-)$	$\sigma(+)$	M_K	$\sigma(-)$	$\sigma(+)$
2MASS J122554–2739A	T6:	I	14.92	.14	.14	14.92	.16	.16	14.73	.20	.20
SDSS J134646–0031	T6	I	15.09	.16	.15	15.16	.17	.16	15.09	.24	.23
SDSS J162414+0029	T6	I+O	15.13	.06	.05	15.21	.07	.06	15.31	.13	.13
2MASS J235654–1553	T6	I	15.05	.12	.12	14.83	.15	.15	14.99	.21	.21
2MASS J104753+2124	T6.5	I	15.71	.13	.13	15.72	.13	.13	15.98	.13	.13
2MASS J123739+6526	T6.5e	I	15.88	.13	.13	15.83	.15	.15	16.06	.23	.23
2MASS J072718+1710	T7	I	15.84	.08	.08	15.94	.18	.18	15.79	.20	.20
2MASS J121711–0311	T7.5	I	16.09	.13	.13	15.95	.17	.17	15.91	.17	.17
2MASS J122554–2739B	T8:	I	16.27	.14	.14	16.27	.16	.16	16.08	.20	.20
2MASS J041519–0935	T8/T9	I	16.92	.07	.07	16.73	.12	.11	16.66	.20	.20

Table 8. Derived L and T Dwarf Bolometric Magnitudes, Luminosities, and T_{eff} .

Star	Sp.T.	$M_{\text{bol}} \pm \sigma(M_{\text{bol}})$	$\log(L/L_{\odot}) \pm \sigma[\log(L/L_{\odot})]$	$T_{\text{eff}} \pm \sigma(T_{\text{eff}})$ (K)
2MASS J034543+2540	L0	13.68 ± 0.14	-3.58 ± 0.06	2426^{+246}_{-191}
SDSS J143517-0046	L0	13.53 ± 1.29	-3.52 ± 0.52	2511^{+915}_{-664}
SDSS J225529-0034	L0:	13.59 ± 0.39	-3.54 ± 0.16	2477^{+338}_{-276}
2MASS J074642+2000A	L0.5	13.84 ± 0.14	-3.64 ± 0.06	2338^{+238}_{-187}
2MASS J143928+1929	L1	13.98 ± 0.14	-3.70 ± 0.06	2264^{+230}_{-181}
2MASS J165803+7027	L1	13.87 ± 0.14	-3.65 ± 0.06	2322^{+236}_{-186}
Kelu-1	L2	13.76 ± 0.16	-3.61 ± 0.06	2382^{+246}_{-195}
DENIS J1058.7-1548	L3	14.79 ± 0.14	-4.02 ± 0.06	1879^{+191}_{-150}
2MASS J114634+2230A	L3	14.39 ± 0.14	-3.86 ± 0.06	2060^{+209}_{-165}
2MASS J143535-0043	L3	14.41 ± 0.84	-3.87 ± 0.34	2051^{+489}_{-386}
2MASS J003616+1821	L3.5	14.69 ± 0.13	-3.98 ± 0.05	1923^{+193}_{-153}
2MASS J032613+2950	L3.5	14.56 ± 0.18	-3.93 ± 0.07	1981^{+209}_{-166}
2MASS J184108+3117	L4pec	14.45 ± 0.23	-3.88 ± 0.09	2032^{+197}_{-181}
2MASS J222443-0158	L4.5	15.09 ± 0.14	-4.14 ± 0.06	1753^{+179}_{-140}
SDSS J053952-0059	L5	15.25 ± 0.15	-4.20 ± 0.06	1690^{+173}_{-137}
DENIS J122815-1547A	L5	15.30 ± 0.16	-4.22 ± 0.06	1671^{+172}_{-137}
DENIS J122815-1547B	L5	15.30 ± 0.16	-4.22 ± 0.06	1671^{+172}_{-137}
2MASS J132855+2114	L5	14.93 ± 0.30	-4.08 ± 0.12	1819^{+197}_{-178}
SDSS J144600+0024	L5	15.51 ± 0.22	-4.31 ± 0.09	1592^{+175}_{-140}
2MASS J150747-1627	L5	15.41 ± 0.13	-4.27 ± 0.05	1629^{+164}_{-129}
SDSS J010752+0041	L5.5	16.04 ± 0.21	-4.52 ± 0.08	1409^{+153}_{-122}
2MASS J085035+1057A	L6	15.81 ± 0.43	-4.43 ± 0.17	1486^{+214}_{-175}
2MASS J095105+3558	L6	14.47 ± 1.10	-3.89 ± 0.44	2023^{+175}_{-175}
2MASS J171145+2232	L6.5	15.64 ± 0.36	-4.36 ± 0.14	1545^{+203}_{-165}
2MASS J003030-1450	L7	15.64 ± 0.31	-4.36 ± 0.12	1545^{+190}_{-154}
2MASS J172811+3948A	L7	16.04 ± 0.22	-4.52 ± 0.09	1409^{+155}_{-124}
DENIS J020529-1159A	L7	15.59 ± 0.15	-4.34 ± 0.06	1563^{+160}_{-127}
DENIS J020529-1159B	L7	15.59 ± 0.15	-4.34 ± 0.06	1563^{+160}_{-127}
SDSS J042348-0414	L7.5/T0	15.28 ± 0.16	-4.22 ± 0.06	1678^{+174}_{-137}
2MASS J082519+2115	L7.5	16.12 ± 0.15	-4.55 ± 0.06	1383^{+142}_{-112}
2MASS J210115+1756A	L7.5	16.30 ± 0.31	-4.62 ± 0.12	1327^{+163}_{-132}
SDSS J003259+1410	L8	15.58 ± 0.41	-4.34 ± 0.16	1566^{+220}_{-179}
2MASS J032842+2302	L8	15.67 ± 0.31	-4.37 ± 0.12	1534^{+189}_{-153}
SDSS J083008+4828	L8	16.30 ± 0.18	-4.62 ± 0.07	1327^{+140}_{-111}
SDSS J132629-0038	L8?	15.84 ± 0.32	-4.44 ± 0.13	1475^{+184}_{-149}
2MASS J152322+3014	L8	16.29 ± 0.19	-4.62 ± 0.08	1330^{+142}_{-112}
2MASS J163229+1904	L8	16.24 ± 0.16	-4.60 ± 0.06	1346^{+139}_{-110}
SDSS J083717-0000	T0.5	16.59 ± 0.93	-4.74 ± 0.37	1241^{+326}_{-252}
SDSS J015141+1244	T1±1	16.43 ± 0.31	-4.68 ± 0.12	1288^{+158}_{-128}
SDSS J125453-0122	T2	16.19 ± 0.19	-4.58 ± 0.08	1361^{+145}_{-115}
SDSS J102109-0304	T3	15.93 ± 0.62	-4.48 ± 0.25	1445^{+267}_{-216}
SDSS J175033+1759	T3.5	15.83 ± 0.37	-4.44 ± 0.15	1478^{+197}_{-160}
SDSS J020742+0000	T4.5	16.63 ± 0.65	-4.76 ± 0.26	1230^{+236}_{-191}
2MASS J055919-1404	T5	15.86 ± 0.17	-4.45 ± 0.06	1469^{+153}_{-122}
2MASS J024313-2453	T6	17.31 ± 0.25	-5.03 ± 0.10	1052^{+119}_{-97}
2MASS J093734+2931	T6p	18.67 ± 0.21	-5.57 ± 0.08	769^{+85}_{-69}

Table 8—Continued

Star	Sp.T.	$M_{bol} \pm \sigma(M_{bol})$	$\log(L/L_{\odot}) \pm \sigma[\log(L/L_{\odot})]$	$T_{\text{eff}} \pm \sigma(T_{\text{eff}})$ (K)
2MASS J122554–2739A	T6:	16.94 ± 0.27	-4.88 ± 0.11	1145^{+133}_{-188}
SDSS J134646–0031	T6	17.30 ± 0.29	-5.02 ± 0.12	1054^{+126}_{-102}
SDSS J162414+0029	T6	17.52 ± 0.20	-5.11 ± 0.08	1002^{+98}_{-86}
2MASS J235654–1553	T6	17.20 ± 0.26	-4.98 ± 0.10	1079^{+124}_{-100}
2MASS J104753+2124	T6.5	18.14 ± 0.20	-5.36 ± 0.08	869^{+93}_{-75}
2MASS J123739+6526	T6.5e	18.22 ± 0.28	-5.39 ± 0.11	853^{+101}_{-82}
2MASS J072718+1710	T7	17.90 ± 0.25	-5.26 ± 0.10	918^{+105}_{-84}
2MASS J121711–0311	T7.5	17.98 ± 0.23	-5.30 ± 0.09	901^{+101}_{-80}
2MASS J122554–2739B	T8:	18.12 ± 0.27	-5.35 ± 0.11	873^{+102}_{-82}
2MASS J041519–0935	T8/T9	18.70 ± 0.26	-5.58 ± 0.10	764^{+88}_{-71}

Table 9. Mean L and T Dwarf Characteristics.

Sp.T.	M_J	M_H	M_K	$J - H$	$J - K$	M_{bol}	$\log(L/L_\odot)$	T_{eff} (K)
L0	11.62	10.85	10.33	0.77	1.29	13.54	-3.52	2510
L0.5	11.81	11.02	10.49	0.79	1.32	13.73	-3.60	2400
L1	12.00	11.19	10.65	0.81	1.35	13.92	-3.67	2300
L1.5	12.19	11.36	10.81	0.83	1.38	14.10	-3.74	2200
L2	12.38	11.54	10.98	0.84	1.40	14.29	-3.82	2110
L2.5	12.57	11.71	11.14	0.86	1.43	14.46	-3.89	2030
L3	12.76	11.88	11.30	0.88	1.46	14.63	-3.96	1950
L3.5	12.95	12.05	11.46	0.90	1.49	14.80	-4.02	1870
L4	13.14	12.22	11.62	0.92	1.52	14.97	-4.09	1800
L4.5	13.33	12.39	11.79	0.94	1.54	15.13	-4.16	1740
L5	13.52	12.57	11.95	0.95	1.57	15.29	-4.22	1670
L5.5	13.71	12.74	12.11	0.97	1.60	15.44	-4.28	1620
L6	13.90	12.91	12.27	0.99	1.63	15.58	-4.34	1570
L6.5	14.09	13.09	12.43	1.00	1.66	15.72	-4.39	1520
L7	14.28	13.26	12.59	1.02	1.69	15.85	-4.44	1470
L7.5	14.47	13.43	12.76	1.04	1.71	15.99	-4.50	1430
L8	14.66	13.60	12.92	1.06	1.74	16.11	-4.55	1390
T0.5	14.79	13.60	13.21	1.19	1.58	16.14	-4.56	1380
T1	14.60	13.58	13.23	1.02	1.37	16.10	-4.54	1390
T1.5	14.44	13.59	13.27	0.85	1.17	16.08	-4.54	1400
T2	14.33	13.63	13.35	0.70	0.98	16.09	-4.54	1390
T2.5	14.27	13.70	13.46	0.57	0.81	16.11	-4.55	1390
T3	14.26	13.80	13.60	0.46	0.66	16.20	-4.58	1360
T3.5	14.28	13.93	13.77	0.35	0.51	16.30	-4.62	1330
T4	14.36	14.10	13.96	0.26	0.40	16.42	-4.67	1290
T4.5	14.48	14.29	14.19	0.19	0.29	16.59	-4.74	1240
T5	14.64	14.52	14.45	0.12	0.19	16.78	-4.82	1190
T5.5	14.85	14.78	14.74	0.07	0.11	17.01	-4.91	1130
T6	15.11	15.07	15.06	0.04	0.05	17.27	-5.01	1060
T6.5	15.41	15.39	15.41	0.02	0.00	17.57	-5.13	990
T7	15.75	15.74	15.79	0.01	-0.04	17.90	-5.26	920
T7.5	16.14	16.12	16.20	0.02	-0.06	18.27	-5.41	840
T8	16.58	16.53	16.64	0.05	-0.06	18.68	-5.58	770